NON-FOURIER HEAT EQUATIONS IN SOLIDS ANALYZED FROM PHONON STATISTICS

A Thesis
Presented to
The Academic Faculty

by

Trevor James Bright

In Partial Fulfillment
of the Requirements for the Degree
Master of Science in the
School of Mechanical Engineering

Georgia Institute of Technology
August 2009

NON-FOURIER HEAT EQUATIONS IN SOLIDS ANALYZED FROM PHONON STATISTICS

Approved by:

Dr. Zhuomin Zhang, Advisor
School of Mechanical Engineering
Georgia Institute of Technology

Dr. G.P. Peterson
School of Mechanical Engineering
Georgia Institute of Technology

Dr. Satish Kumar
School of Mechanical Engineering
Georgia Institute of Technology

Date Approved: 06/28/2009

ACKNOWLEDGMENTS

I would like to express my gratitude to Dr. Zhuomin Zhang for his guidance over the past semesters allowing this work to become a reality. He has taught me a great deal about professionalism and quality (and life in general) and hopefully I can continue to maintain as high a standard as he has for his students throughout the rest of my life and career. I would also like to thank Dr. Bud Peterson and Dr. Satish Kumar for taking the time to serve on my committee and their valuable advice and comments.

In addition I would like to show my deepest appreciation to the Nanoscale Radiation Heat Transfer Group at the Georgia Institute of Technology for their help and encouragement. In particular Xiaojia Wang, Andrew McNamara, and Liping Wang for their support and friendship during my study at Georgia Tech. I am indebted to Mr. Soumya Basu and Dr. Bong Jae Lee for their good advice regarding graduate studies as well as their friendship. I was very lucky to have such outstanding colleagues during my study.

Finally, I would like to thank my family for their love and support which I am truly fortunate to have. Without them none of this would have been possible.

TABLE OF CONTENTS

LIST OF TABLES

LIST OF FIGURES

LIST OF SYMBOLS

$\mathbf{a}$	acceleration vector
c_p	specific heat capacity
D	density of state
f	distribution function
f_0	equilibrium distribution function
$\hbar$	Planck's constant divided by 2π
I_ω	radiative intensity at a given frequency
I	radiative intensity integrated over all frequencies
I_ω^0	equilibrium intensity at a given frequency
k	thermal conductivity
k_B	Boltzmann constant
L	distance between walls
L_ω	entropy intensity
$\mathbf{q}''$	heat flux vector

q''_x	heat flux in the x direction
$\dot{q}$	volumetric heat generation
$\mathbf{r}$	position vector
$\dot{s}_{\text{gen}}$	volumetric entropy generation
s''_{gen}	wall entropy generation
s''_{tot}	combined wall and medium entropy generation
S	nondimensional heat source term
t	time
T	temperature
T^*	equilibrium temperature of medium
T_ω	brightness temperature
$\mathbf{v}$	velocity vector
v	magnitude of velocity or speed
v_a	speed of sound
v_g	group velocity

v_p phase velocity

x position

Greek Symbols

α thermal diffusivity

γ non-dimensional position

ζ similarity parameter

θ dimensionless temperature

η dimensionless position

Λ mean free path

μ direction cosine

ξ dimensionless time

ρ density

σ'_{SB} phonon Stefan-Boltzmann constant

τ relaxation time

ω	angular frequency

Subscripts

1	left wall (low temperature)
2	right wall (high temperature)
M	medium between two black walls
s	surface
tw	temperature wave (commonly known as thermal wave)

SUMMARY

Advances in microelectronics and nanotechnology have generated tremendous interest in the non-Fourier regimes of heat conduction, where the conventional theories based on local equilibrium no longer apply. The non-Fourier regimes include small length scales, where the medium can no longer be treated using bulk properties, and short time scales, on the order of the relaxation time of heat carriers. One of the objectives of this thesis is to clarify some misunderstandings of the hyperbolic heat equation (HHE), commonly thought of as a remedy of Fourier's law at short time scales. The HHE is analyzed from the stand point of statistical mechanics with an emphasis on the consequences of the assumptions applied to the Boltzmann transport equation (BTE) when deriving the HHE. In addition, some misperceptions of the HHE, caused by a few experiments and confusion with other physical phenomena, are clarified. It is concluded that HHE should not be interpreted as a more general equation governing heat transport because of several fundamental limitations. The other objective of this thesis is to introduce radiation entropy to the equation of phonon radiative transport (EPRT) for understanding the heat conduction mechanism on a fundamental level which can be applied to both diffusion and ballistic heat transport in dielectric solids. The entropy generation due to phonon transport is examined along with the definition of a phonon brightness temperature, which is direction and frequency dependent. A better understanding of non-Fourier heat conduction will help researchers and engineers to choose appropriate theories or models in analyzing thermal transport in nanodevices.

CHAPTER 1

INTRODUCTION

Growing interest in devices on the order of nanometers has resulted in the need to understand heat transport at small scales. The physics that govern heat transport are largely dependent on how energy carriers interact with each other, defects inside of the medium, and boundaries. Electrons, despite their particle nature, propagate as waves inside of a medium and thus are able to travel reasonable well through a periodic crystal lattice. Phonons, on the other hand, are the quantum particle representation of lattice vibration propagating through a medium and are also capable of transporting and redistributing energy spatially inside of a medium. Defects such as missing atoms or non-basis atoms can disturb the propagation of electrons and phonons resulting in defect scattering. In addition electron waves and phonon waves can interact with each other or other waves of the same type resulting in electron-phonon scattering, phonon-phonon scattering and electron-electron scattering mechanisms to redistribute thermal energy throughout the medium. In addition the boundaries between two media in direct contact, with different properties, can cause boundary scattering of electrons and phonons. For larger scales, both temporal and spatial, the interactions between carriers are described macroscopically by traditional equations such as Fourier's law which relates the temperature gradient inside of a medium to the flux of heat in any direction. In the past Fourier's law was adequate in most situations however new technologies such as short laser pulses which are on the order of picoseconds and new fabrication methods allowing

the deposition of thinner and thinner films onto substrates, which have applications in electronics, have generated a need to understand heat transfer in new regimes which have only recently become of importance

Fourier's law has long been established as the governing law of heat conduction, describing the thermal energy propagation in a medium via a diffusion process. It has served as a reliable model for predicting the temperature in a medium, as well as the rate of heat propagation through a medium, that has been validated by numerous experiments. One of the predicted results of Fourier's law, as with all diffusion processes, is that the effect of a source will be instantaneously felt everywhere in a medium, although such a nonzero effect is practically negligible at large distances. Since heat is carried by particles such as electrons, and quanta such as phonons, which are forbidden to propagate at speeds greater than that of light, it is impossible that the response to a sudden heat flux at one location in a medium should be instantaneously felt at all other locations within the medium. This paradox has spurred much academic interest in the last half century towards seeking a model that can predict a finite speed of propagation [1-5].

The short comings of Fourier's law have divided heat conduction into several regimes which need to be treated differently when modeling thermal transport. Macroscopic equations such as the hyperbolic heat conduction equation (HHE) are intended to extend our traditional understand of conduction to shorter time scales where insufficient time has elapsed to describe heat transport by Fourier's law. This sort of macroscopic equation is expressed in terms of the temperature and can be solved to give the temperature distribution directly. Other models such as the equation of phonon radiative transport (EPRT) can be solved to determine the particle distribution function

and from the distribution function the effective temperature of the medium can be determined. Rigorously speaking the definition of temperature is not the same in non-Fourier heat conduction as the traditional definition based on the zeroth law of thermodynamics.

Much work has been done on generating and solving models that describe non-Fourier heat conduction [3, 6, 7]. Many of the proposed models are based on the Boltzmann transport equation (BTE) which is viewed by many researchers as a more fundamental equation describing transport phenomenon that can be extended to short time and length scales. The HHE and EPRT are two such models based on simplification of heat carrier scattering term in the BTE. In order to improve the current understanding of heat transfer as a nonequilibrium phenomenon in the non-Fourier regime this work analyses the HHE as derived from the BTE. Starting from the physical limitation imposed by the underlying approximations used to derive the HHE. The EPRT is solved for a 1D medium and the solutions are analyzed from an original perspective. In addition a second law perspective is taken with the EPRT and entropy generation is analyzed from the more fundamental BTE by applying concepts for traditional radiation heat transport to phonon radiative transport. This work will contribute to the understanding of modeling heat transport in the non-Fourier regimes of heat transport by clarifying common misperceptions of the HHE and analyzing entropy generation at short length scales using the EPRT.

This thesis is organized into five chapters as follows: Chapter 1 gives the importance, background, problem, approach, and contributions of this work. Chapter 2 gives a theoretical overview of non-Fourier heat transport. Chapter 3 clarifies some

common misperceptions of the HHE with some new physical insight. Chapter 4 extends the concept of radiation entropy to entropy generation in phonon radiative transport, and offers new perspectives on phonon conduction. Chapter 5 concludes the present work and outlines some future directions in the area of non-Fourier heat transport.

CHAPTER 2

THEORETICAL BACKGROUND

Non-Fourier heat transfer models attempt to describe heat transfer macroscopically based on fundamental microscopic descriptions of heat carriers. The HHE and the EPRT, two common models for non-Fourier heat transfer, are derived from the classical BTE. The BTE is a fundamental transport theorem and a brief description of the BTE is presented in this chapter. In addition the following sections present the fundamental background for the HHE and EPRT based on their derivation from the BTE.

2.2 Overview of the Boltzmann Transport Equation

Heat transfer in the non-Fourier regime is generally based on analysis of the BTE which can be used to determine the evolution of the distribution function for electrons, photons, and phonons. Based on the kinetic theory of particles Boltzmann was able to derive the BTE for the distribution function of a single particle. In the absence of collision the probability of finding a particle with initial velocity $\mathbf{v}$ and position $\mathbf{r}$ at time $\mathbf{t}$ under an acceleration $\mathbf{a}$ due to a body force $\mathbf{F}$ will be the same as the probability of finding a particle with velocity $\mathbf{v}+\mathbf{a}dt$ and position $\mathbf{r}+\mathbf{v}dt$ at time $t+dt$ giving

$$\frac{f\left(\mathbf{r}+\mathbf{v}dt,\mathbf{v}+\mathbf{a}dt,t+dt\right)-f\left(\mathbf{r},\mathbf{v},t\right)}{dt}=\frac{\partial f}{\partial t}+\mathbf{v}\cdot\frac{\partial f}{\partial \mathbf{r}}+\mathbf{a}\cdot\frac{\partial f}{\partial \mathbf{v}}=0 \qquad (2.1)$$

Boltzmann proposed the addition of a collision term on the right hand side giving the following equation known as the Botlzmann transport equation:

$$\frac{\partial f}{\partial t} + \mathbf{v} \cdot \frac{\partial f}{\partial \mathbf{r}} + \mathbf{a} \cdot \frac{\partial f}{\partial \mathbf{v}} = \left[\frac{\partial f}{\partial t} \right]_{\text{coll}} \tag{2.2}$$

The collision term can be quite complicated and in the absence of multi-body collisions under the molecular chaos assumption can be modeled as [8]

$$\left[\frac{\partial f}{\partial t} \right]_{\text{coll}} = -\int W_{(\mathbf{p},\mathbf{p}_2 \to \mathbf{p}_1',\mathbf{p}_2')} \left(f f_2 - f_1' f_2' \right) d\mathbf{p}_2 d\mathbf{p}_1' d\mathbf{p}_2' \tag{2.3}$$

where $W_{(\mathbf{p},\mathbf{p}_2 \to \mathbf{p}_1',\mathbf{p}_2')}$ is the probability that a collision between a particle with momentum $\mathbf{p}$ colliding with a particle of momentum $\mathbf{p}_2$ producing particles with momentums of $\mathbf{p}_1'$ and $\mathbf{p}_2'$ per unit time. The first term on the left side of the parenthesis represents out-scattering (a reduction in the number density of at a given momentum) and the second term represents in scattering (increase in the number density at a given momentum). Since integration must be performed to account for all the possible momentums of the second particle and the two outgoing particles the resulting integro-differential equation is troublesome. In addition the scattering probability may depend on the nature of the scattering etc. Typically simplifying assumptions are made the BTE in order to extract a solution and some typical simplifications will be discussed in the next section.

2.3 Approximations in the Boltzmann Transport Equation

The BTE in the un-simplified form contains a generic collision term to describe the time rate of change of a single particle distribution function due to collisions. It is through collisions that energy is redistributed and the distribution function of a single particle is returned to the equilibrium distribution function. It should be noted that the BTE is a single particle distribution function, as opposed to the Liouville equation which

is an N-particle distribution function, and is not the most fundamental description of transport phenomenon since it neglects certain particle wave effects [8]. The BTE however is not as limited in its application as the classical equations which describe heat transport as it can be applied at short time and length scales and under the appropriate simplifications can be used to derive classical expressions such as Fourier's law. The BTE can be considered as more fundamental in the sense that it is more general and its application overlaps heat transfer regimes.

The most common approximation in the heat transfer community is the relaxation time approximation, which is given mathematically by

$$\left[\frac{\partial f}{\partial t}\right]_{\text{coll}} = \frac{f_0 - f}{\tau(\mathbf{v})} \tag{2.4}$$

Here, the term f_0 signifies the equilibrium distribution and $\tau(\mathbf{v})$ is the relaxation time, which is in general dependent on the velocity or momentum of the particles. A further assumption is made that the relaxation time is independent of velocity, denoting the average relaxation time by τ_{q} for convenience. Under the relaxation time approximation the rate of change of the non-equilibrium distribution function is proportional to the difference between the equilibrium and non-equilibrium distribution function and collisions are the driving force that returns the distribution function to an equilibrium state. The relaxation time approximation is thus a linearization of the collision term and in order to be valid any non-linear effects of collisions must be negligible. The relaxation time approximation is limited in this sense to time scales greater than the relaxation time since at shorter times particle have not had sufficient time to interact, in addition at short time scales higher order effects of collisions will be more important.

Another important assumption is called the local equilibrium assumption. Consider a one-dimensional problem where the temperature gradient is in the *x* direction only. This assumption can be expressed as follows [9]:

$$\frac{\partial f}{\partial x} \approx \frac{\partial f_0}{\partial x} \tag{2.5}$$

The local equilibrium assumption implies that the spatial derivative of the nonequilibrium distribution can be approximated as that of the equilibrium distribution. Generally speaking the local equilibrium approximation requires that temperature deviation (temperature gradient) over a mean free path not be too large. More discussion of the simplifying assumptions used to derive heat transport equations will follow in the subsequent chapters.

2.4 The Hyperbolic Heat Conduction Equation

After applying the relaxation time and local equilibrium approximations and dropping the acceleration term the 1D BTE becomes

$$\frac{\partial f}{\partial t} + v_x \frac{\partial f_0}{\partial x} = \frac{f_0 - f}{\tau} \tag{2.6}$$

Here, v_x is the *x*-component of the velocity, f is the actual distribution function (in terms of frequency) and is usually anisotropic at given *x* and *t*, f_0 is the equilibrium distribution function, and τ is the relaxation time that is in general a function of frequency and phonon velocity. After some manipulation and integrating over the entire velocity, $\mathbf{v}$, space Eq. (2.6) can be expressed as

$$\frac{\partial}{\partial t}\int_{\mathbf{v}} \tau v_x f \varepsilon d\mathbf{v} + \int_{\mathbf{v}} \tau v_x^2 \frac{\partial f_0}{\partial T}\frac{\partial T}{\partial x} \varepsilon d\mathbf{v} = -\int_{\mathbf{v}} v_x f \varepsilon d\mathbf{v} \tag{2.7}$$

Equation (2.7) gives rise to the following rate equation for heat flux which is known as Cattaneo's equation or sometimes referred to as the Cattaneo-Vernotte equation [1, 2]:

$$\mathbf{q}'' + \tau_q \frac{\partial \mathbf{q}''}{\partial t} = -k\nabla T \tag{2.8}$$

This equation differs from the classical Fourier's law with the addition of the second term on the left hand side. At longer time scales this additional term becomes negligible and Eq. (2.8) reduces to Fourier's law. If the constant τ_q were negligibly small compared with the characteristic time, then this term would be removed and the equation would reduce to Fourier's law. The value of τ_q in Eq. (2.8) is generally taken to represent some average thermal relaxation time since there may be different relaxation times associated with various carriers in a medium. Physically the thermal relaxation time is a measure of the average time between two successive collisions of the heat carriers in a medium. It has been proposed that Cattaneo's equation is more general than Fourier's law and is valid at shorter time scales, as the heat flux is not assumed to be established instantaneously but with a time delay. As early as 1867, Maxwell derived an equation similar to Eq. (2.8) based on gas dynamics. By assuming that the time rate of change of the heat flux would be negligible as the heat flux would establish itself very rapidly, Maxwell was then able to obtain Fourier's law from a microscopic viewpoint after dropping the time derivatives. Cattaneo derived Eq. (2.8) in 1948 using kinetic theory and extended it to demonstrate the finite propagation speed of heat in 1958. Later, others also derived Eq. (2.8) from the Boltzmann transport equation (BTE) [10] under the relaxation time assumption for phonon and electron transport. All the derivations made improper assumptions and do not

justify the application of Eq. (2.8) to very short time scales, as will be elaborated in the next chapter.

The HHE can be arrived at by combining Eq. (2.8) with the energy equation for an elemental control volume:

$$\dot{q} - \nabla \cdot \mathbf{q}'' = \rho c_p \frac{\partial T}{\partial t} \tag{2.9}$$

Equations (2.8) and (2.9) can be combined to yield

$$\frac{\dot{q}}{k} + \frac{\tau_q}{k}\frac{\partial \dot{q}}{\partial t} + \nabla^2 T = \frac{1}{\alpha}\frac{\partial T}{\partial t} + \frac{\tau_q}{\alpha}\frac{\partial^2 T}{\partial t^2} \tag{2.10}$$

which is the HHE with generation. Without heat generation, it can be simplified to

$$\nabla^2 T = \frac{1}{\alpha}\frac{\partial T}{\partial t} + \frac{\tau_q}{\alpha}\frac{\partial^2 T}{\partial t^2} \tag{2.11}$$

Equation (2.11) is a damped-wave equation with a wave propagation speed given by

$$v_{\mathrm{tw}} = \sqrt{\alpha / \tau_q} \tag{2.12}$$

HHE predicts a wave, whose amplitude corresponds to the temperature in a medium, that will propagate through a medium at the speed of v_{tw} and its amplitude will decay rapidly as it propagates. This speed is finite as long as $\tau_q \neq 0$, indicating that the thermal signal cannot be felt at locations beyond the wave front. If τ_q is taken to be equal to the relaxation time of heat carriers, and the value of thermal conductivity is estimated from simple kinetic theory [11], then it can be shown that

$$v_{\mathrm{tw}} = v_{\mathrm{g}} / \sqrt{3} \tag{2.13}$$

where v_{g} is the group velocity (either the Fermi velocity for electrons or the speed of sound for phonons).

2.5 The Equation of Phonon Radiative Transport

The EPRT can be used to model heat conduction in thin films as shown schematically in Figure 2.1. EPRT models conduction inside of thin films based on the BTE with the relaxation time approximation. Heat conduction is said to be radiative under EPRT due to the similar form and definition of the governing equation to the radiative transfer equation (RTA) which governs radiative heat transfer in a participating medium.

The 1D BTE under the relaxation time approximation can be expresses as follows [7, 9, 12]

$$\frac{\partial f}{\partial t} + v_x \frac{\partial f}{\partial x} = \frac{f_0 - f}{\tau} \tag{2.14}$$

by neglecting the acceleration term. Note the difference between Eq. (2.6) and Eq. (2.14) is the local equilibrium approximation has been made in Eq. (2.6). For phonons, the equilibrium distribution function is given by the Bose-Einstein statistics that is a function of temperature and frequency but not the direction (i.e., isotropic).

Based on the energy flux a phonon intensity can be defined that is consistent with the intensity as defined in the case of radiation. The intensity of a phonon in a given direction at a single frequency is given by [9]

$$I_\omega(\omega,\theta,\phi)=\frac{1}{4\pi}\sum_P v_g \hbar\omega f D(\omega) \tag{2.15}$$

where $\hbar$ is Planck's constant divided by 2π, the density of state $D(\omega)$ represents the number of vibration modes between ω and $\omega+d\omega$ per unit volume, and v_g is the group velocity in the direction defined by the zenith angle θ and azimuthal angle ϕ. Since the energy of a single phonon is $\hbar\omega$, Eq. (2.15) represents the rate of heat transfer per unit projected area, per solid angle, and per unit frequency interval, just as in the case of photon radiation. Based on this definition of phonon intensity, the heat flux in the x direction can be evaluated from the phonon intensity using

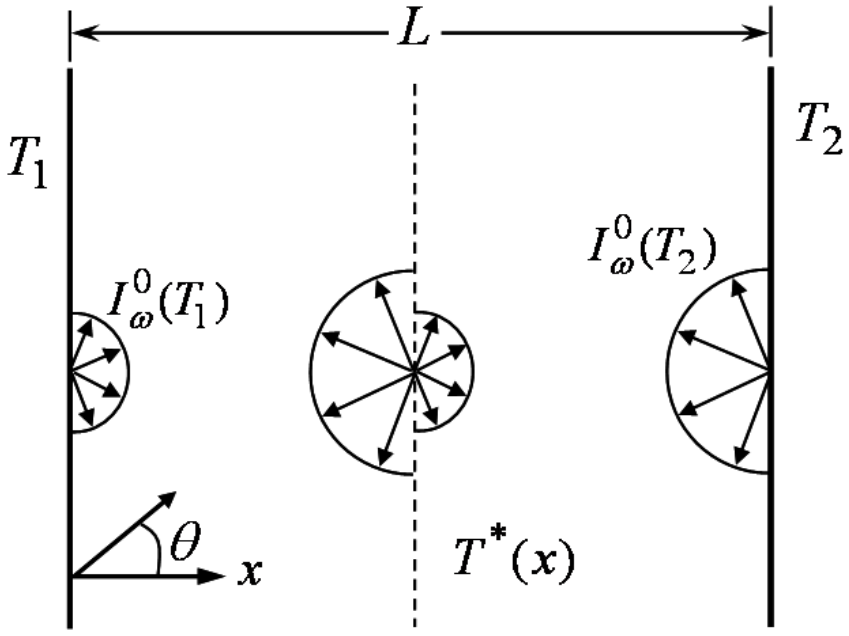

Fig. 2.1 Schematic showing directional intensity distribution at a single frequency inside a medium between two black walls at temperatures T_1 and T_2. The intensity at a vertical plane inside of the medium (dashed line) is shown qualitatively for $T_2 > T_1$ in the acoustically thin limit. Each wall acts as a thermal reservoir at a constant temperature, thus heat is transported as a radiation process inside of the medium.

$$q''_x = \int_0^\infty q''_\omega d\omega = 2\pi \int_0^\infty \int_{-1}^{1} \mu I_\omega(\mu,\omega)\, d\mu d\omega \tag{2.16}$$

where $\mu = \cos(\theta)$ is the direction cosine relative to the x direction (see Fig. 2.1), and q''_ω is the spectral heat flux. It is assumed that the intensity is not a function of the azimuthal angle ϕ. The phonon equilibrium intensity can be derived from the Bose-Einstein distribution function, which gives [9]

$$I^0_\omega(\omega,T) = \sum_P \frac{\hbar\omega^3}{8\pi^3 v_{\mathrm{p}}^2 \left(e^{\hbar\omega/k_{\mathrm{B}}T} - 1\right)} \tag{2.17}$$

where the summation is taken over the two transverse and one longitudinal phonon polarizations, and v_{p} is the phase speed for the corresponding polarization. Assume that the phonon dispersion is linear and an average acoustic speed (i.e., the sound velocity) v_{a} can be used for all three polarizations. Then, the equilibrium intensity becomes

$$I^0_\omega(\omega,T) = \frac{3\hbar\omega^3}{8\pi^3 v_{\mathrm{a}}^2 \left(e^{\hbar\omega/k_{\mathrm{B}}T} - 1\right)} \tag{2.18}$$

Note that emission of phonon from a black wall has the intensity equal to the equilibrium intensity that is by definition independent of the direction cosine. Substituting Eq. (2.15) into Eq. (2.14) and noting that $v_x = v_{\mathrm{a}} \cos\theta$, one obtains the EPRT at steady state [7]

$$\mu \frac{dI_\omega}{dx} = \frac{I^0_\omega(\omega,T^*) - I_\omega}{v_{\mathrm{a}}\tau} \tag{2.19}$$

Equation (2.19) is very similar to the radiative transfer equation (ERT) for electromagnetic radiation in an absorbing and emitting medium with no scattering. Scattering of phonons by crystalline defects and other phonons is analogous to the emission and absorption processes in the conventional ERT. Unlike ERT for a gas

medium, $T^*(x)$ in Eq. (2.19) is an *effective* temperature of the medium. Rigorous speaking, a thermodynamic temperature cannot be defined in the medium unless the thickness of the film L is much greater than the phonon mean free path, $\Lambda = v_a \tau$. The Knudsen number given by

$$Kn = \frac{\Lambda}{L} \tag{2.20}$$

is a parameter that characterizes the acoustic thickness of the medium. A large *Kn* implies the acoustically thin limit known as Casimir's limit [13], whereas a very small *Kn* implies the diffusion limit where Fourier's law can be applied. Only in the acoustically thick limit, the effective temperature $T^*(x)$ becomes the local equilibrium temperature in the conventional sense. A further assumption is made such that the relaxation time is independent of the frequency, i.e., the gray-medium assumption, since the inverse of the mean free path is analogous to the absorption coefficient in photon radiative transfer.

CHAPTER 3

MISPERCEPTIONS OF THE HYPERBOLIC HEAT EQUATION

The current chapter aims at clarifying some common misperceptions of HHE in a systematic manner, with additional new insights into the microscopic theory of heat carriers and the paradox of infinite propagation speed. A brief description of HHE and its associated characteristics are given first. Then, the PHE and HHE are considered within statistical mechanics, classical thermodynamics, and irreversible thermodynamics frameworks. The lack of soundness of the well cited works that offer misleading experimental evidence to support HHE is also addressed.

3.1 Assumptions Used in Deriving the Hyperbolic Heat Equation

As mentioned in Chapter 2, HHE can be derived from BTE, which describes the evolution of the nonequilibrium distribution of particles in the phase space. The distribution function f describes the probability of a particle occupying a given quantum state; it is assumed that the energy levels are sufficiently dense to allow the energy distribution to be treated as if it were continuous. BTE itself has two limiting assumptions; namely, particle reactions are infrequent and the wave nature of particles can be neglected. Such conditions apply for substances such as ideal gases. Nevertheless, BTE is valid for all time and length scales and can be expressed as [9]

$$\frac{\partial f}{\partial t} + \mathbf{v} \cdot \frac{\partial f}{\partial \mathbf{r}} + \mathbf{a} \cdot \frac{\partial f}{\partial \mathbf{v}} = \left[\frac{\partial f}{\partial t} \right]_{\text{coll}} \tag{3.1}$$

The last term on the right represents the effect of molecular collisions that restore the distribution function to its equilibrium state. BTE provides a method by which one can determine the behavior of nonequilibrium distributions. This is critical since heat transfer will only occur as a result of a nonequilibrium distribution. Furthermore, BTE is not limited to just gasses, but can be extended to other particles and quanta that can be modeled as having infrequent interactions and obey certain distribution functions. The behavior of these particles must have some features in common with an ideal gas; thus, the term electron gas and phonon gas have been coined to describe the behavior of heat carriers in a solid medium. Cattaneo's equation can be derived from the BTE by applying the relaxation time assumption, which linearizes the collision term by assuming that the system is not too far from equilibrium.

However the derivation of HHE from BTE after these assumptions is not sufficient to justify HHE, since the assumption of local equilibrium does not apply to a system subject to a disturbance shorter than relaxation time when particles do not have sufficient time to interact. In fact, the HHE and the PHE are subject to the same limitation at short time scales: both are not applicable to time scales shorter or close to the relaxation time. At longer time duration when $t >> \tau_q$, the HHE and PHE are essentially the same. Several theoretical studies have showed that neither HHE nor PHE can predict the transient behavior at short time scales for phonon or electron systems [14-16]. The statement that HHE is applicable at short time scales, as long as the characteristic length is much larger than the mean free path, is misleading. The propagation distance of the wave front during one relaxation time falls in the regime of micro-length scales as elaborated in the next section. Thus, local equilibrium cannot be guaranteed and HHE is

not appropriate for use at time scales shorter or close to the relaxation time, which is the regime that the HHE was intended to be applied to improve the PHE.

3.2 The Wave Behavior of the Hyperbolic Heat Equation

If the temperature distribution in a medium does in fact obey HHE (a damped wave equation), then many phenomena associated with waves should be observed in the form of temperature waves across a medium. One feature of temperature waves according to HHE would be a sharp wave front and wavelike temperature distribution, induced by a heat pulse with a duration smaller than or on the order of the relaxation time. The wave front could have an amplitude much higher than the temperatures predicted by PHE and would decay as it travels through the medium redistributing the thermal energy. After a time period much longer than τ_q, the temperature distribution predicted by HHE would eventually settle to the one predicted by PHE. To illustrate the concept of temperature wave, let us consider a 1D slab of finite thickness L with internal heat generation. The governing HHE becomes

$$\frac{1}{v_{\text{tw}}^2}\frac{\partial^2 T}{\partial t^2}+\frac{1}{\alpha}\frac{\partial T}{\partial t}=\frac{\partial^2 T}{\partial x^2}+\frac{1}{k}\left[\dot{q}(x,t)+\frac{\alpha}{v_{\text{tw}}^2}\frac{\partial \dot{q}(x,t)}{\partial t}\right] \tag{3.2}$$

The solution of this equation has been given by Özişik and Vick [17] in terms of dimensionless variables. The dimensionless position η and time ξ are defined as

$$\eta=\frac{v_{\text{tw}}x}{2\alpha} \text{ and } \xi=\frac{v_{\text{tw}}^2 t}{2\alpha} \tag{3.3}$$

A nondimensional source term is defined as

$$S(\eta,\xi)=\frac{4\alpha^2\dot{q}}{q_0 v_{\text{tw}}^3} \tag{3.4}$$

where q_0 represents the total energy generation over the entire slab for time from 0 to infinity:

$$q_0 = \int_0^\infty \int_0^L \dot{q}(x,t)\,dxdt \tag{3.5}$$

Consider the case of short pulse laser heating of a medium. A very rapid laser pulse can be modeled as an instantaneous release of energy. Such a pulse can be represented by a piecewise dimensionless generation function that originated from a nondimensionless thickness $\Delta\eta$ and becomes zero for $\eta > \Delta\eta$.

$$\Delta\eta = \frac{v_{\text{tw}}\Delta x}{2\alpha} \tag{3.6}$$

and

$$S(\eta,\xi) = \begin{cases} \dfrac{1}{\Delta\eta}\delta(\xi), & 0 \le \eta \le \Delta\eta \\ 0, & \Delta\eta < \eta \le \eta_L \end{cases} \tag{3.7}$$

where η_L corresponds to the boundary at $x = L$. The Dirac delta function is used to model the thermal energy generation as occurring instantaneously with all the energy released at $t = 0$. In essence, $\Delta\eta$ represents a region near the surface of the wall where the laser pulse is modeled as a generation term. Note that both boundaries are assumed to be adiabatic. Green's function method was used to arrive at the following solution for a single pulse [17].

$$\begin{aligned} \theta(\eta,\xi) = {} & \frac{1}{2\eta_L} + \frac{1}{\eta_L} e^{-\xi} \sum_{m=1}^{\infty} \cos(\lambda_m \eta) \\ & \times \frac{\sin(\lambda_m \Delta\eta)}{\lambda_m \Delta\eta} \left[\frac{\sin\left(\xi\sqrt{\lambda_m^{\,2}-1}\right)}{\lambda_m^{\,2}-1} + \cos\left(\xi\sqrt{\lambda_m^{\,2}-1}\right) \right] \end{aligned} \tag{3.8}$$

where $\theta = k\Delta T / q_0 v_{tw}$ is a dimensionless temperature with ΔT being the temperature rise with respect to the initial temperature, and the eigenvalues for the series are given by $\lambda_m = m\pi / \eta_L$.

The solution of Eq. (3.8) is illustrated in Fig. 3.1 at three dimensionless time values. The direction of wave propagation is indicated by the arrow and the decaying amplitude of the wave front. After the temperature wave front reaches the boundary, it is reflected back in the opposite direction. The wave continues to decay on each pass until the solution becomes the same as that predicted by PHE.

In addition to the propagation and reflection of thermal waves the possibility of resonance features of the wave in response to various source frequencies has also been

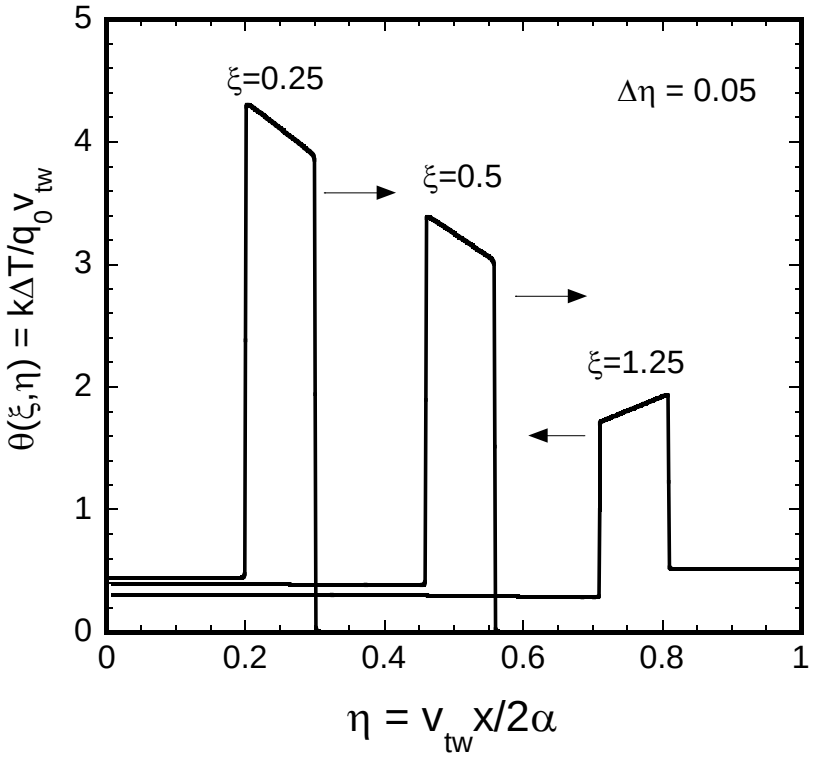

Figure 3.1: Propagation of temperature wave in medium due to pulse heat source with duration less than the relaxation

investigated. Tzou [18] studied the resonance phenomenon for thermal waves and predicted the critical frequency of resonance. Two thermal waves may interfere constructively or exhibit resonance features similar to mechanical waves. In addition to resonance the wave may experience reflection as discussed previously, as well as refraction at the boundaries when adiabatic boundary conditions are removed. Most publications on HHE dealt with numerical or analytical solutions with very few experimental studies that are questionable as will be discussed later in this chapter.

From this wave example, which is used to model short pulse laser heating, one can see why local equilibrium condition and relaxation time approximation are not satisfied by observing the solutions of HHE as shown in Fig. 3.1. The solution has a very sharp wave front with an elevated temperature. The simplification of the collision term (relaxation time approximation) used to derive the HHE relies on a linear behavior of scattering. Such an approximation relies on the distribution function being not too far from equilibrium, otherwise one should use the more general collision term in the BTE since the BTE used to derive the HHE may not govern all heat carriers inside of the medium. The sharp wave front will result in collisions between particles of different energies and a jump in the equilibrium distribution function at that location invalidating the simplifying approximations. Particles ahead of this wave front will still have an undisturbed equilibrium distribution while particles at the wave front will be in a state of nonequilibrium with an elevated temperature. The wave front will pass through this region and the particles occupying the region will then experience a sudden jump in temperature. Obviously, there is no way to establish local equilibrium at the front and back end of the pulse. When modeling the medium using BTE there is no reason to think

that the approximations should be applicable throughout the medium (due to the single particle nature of BTE) if a large disturbance should propagate through the medium with a sharp wave front. Körner and Bergmann [19] showed that for three-dimensional problems involving a point heat source, HHE can result in nonphysical solutions, such as a local negative energy value and temperature below absolute zero. Many also showed that HHE could predict results that contradict the second law of thermodynamics as will be discussed in the next section.

3.3 Statistical Perspective of Thermal Transport

An apparent advantage of HHE is the removal of the paradox of infinite speed of propagation associated with Fourier's law. It is interesting to note that the classical and quantum statistics of particles do not explicitly limit the speed at which particles travel. The probability of gas particles and free electrons in their statistical models allows large velocities with a probability approaching zero as the velocity goes to infinity. The statistical model of phonons, however, will have a finite velocity limit that depends on the speed of sound in the material but derivations of the HHE should be valid without ever considering the heat carrier type as discussed later. The free path distribution allows for a particle to travel extremely large distances without colliding with another particle with a very small probability. Take for instance the Maxwell-Boltzmann distribution; the probability is nonzero for a particle to travel faster than the speed of light, albeit the probability is extremely small. Any particle traveling at a finite speed, even if that speed is greater than the speed of light, has a small probability of having a relaxation time long enough to allow a miniscule but nonzero effect at very large distances. Under the well-

accepted statistical models, heat could propagate at an unbounded rate, although the probability of carriers propagating at extremely high rate decreases to nearly zero. The limitation is set by the negligible probability; hence, these statistics will not predict any meaningful heat propagation at a speed greater than the speed of light that will contradict the special theory of relativity. A finite but negligibly small change is exactly what should be expected by any equation that is consistent with the statistical models of particles. This is essentially the prediction of Fourier's law which states that the instantaneous response to a thermal disturbance at an infinite distance is not zero but infinitesimally small. It is PHE, rather than HHE, that gives results that are fundamentally consistent with statistical mechanics. In fact HHE does not take into account the type of heat carrier distribution function and always predicts a finite speed of propagation. The wave nature of the HHE on the other hand is more artificial and is partially a consequence of assuming that all particles collide at a distance of a mean free path rather than obey a path distribution function, This is not an issue in the PHE as the relaxation time term has gone to zero.

Note that Fourier's law is only an approximate model of heat transfer that describes the diffusion processes in a single-phase material not involving phase change, advection, or bulk flow. Moreover, all measurements of temperature and heat flux are subject to instrumental uncertainties as well as random noises existing everywhere in nature. The statement that Fourier's law predicts an infinite speed of propagation is strictly limited to the sense of an infinitely small temperature change. The thermal response predicted by Fourier's law decays rapidly toward large distances to below any meaningful values. A more reasonable definition of the speed of heat propagation is the

diffusion speed, which is generally much lower than the thermal wave speed given in Eq. (2.12) as to be elaborated in Sec. 3.6.

3.4 Thermodynamic Considerations

The zeroth law of thermodynamics states that two bodies that are in thermal equilibrium with a third body are in thermal equilibrium with each other. This statement implies the existence of a property of the system known as temperature. This definition of temperature requires that the particles in a body are in a state of interaction with one another. A single particle in the body possesses energy but the temperature of a single particle cannot be defined. Within any given medium, particles will distribute themselves at different energy levels depending on the temperature. Temperature in this sense only posses meaning on scales large enough to define an average energy of particles and only when there is sufficient interaction between particles to define a macroscopic temperature. Therefore, local equilibrium is essential for the definition of thermodynamic temperature to apply [8].

In this sense, the meaning of temperature described in HHE does not satisfy the definition of temperature in thermodynamics. Note that τ_q is a measure of interaction in the medium and presumably to be the same or at least on the same order of the relaxation time in the medium. At time scales near or less than τ_q, there is simply insufficient time for particle interactions to establish themselves. A nonequilibrium temperature can be defined based on the energy of the particles but this is different from the definition of temperature and such a temperature cannot be measured by conventional means such as a thermocouple or electrical resistance thermistor. Many researchers did not make this

distinction between the thermodynamic temperature and nonequilibrium temperature when studying HHE and the associated phenomena.

If the temperature in HHE were taken in the classical sense there could be a negative entropy generation according to classical thermodynamics, which is in violation of the second law. In some cases, HHE may predict a heat transfer from the cold region to the hot region [20]. Barletta and Zanchini [21] derived an expression for the rate of entropy generation based on Eq. (2.8) using classical thermodynamics definitions:

$$\dot{S}_{\text{irr}} = \frac{1}{kT^2}\mathbf{q}'' \cdot \left(\mathbf{q}'' + \tau_{\text{q}} \cdot \frac{\partial \mathbf{q}''}{\partial t} \right) \tag{3.9}$$

When the heat flux decreases rapidly enough with respect to time, Eq. (3.9) will take on a negative value, which is forbidden in classical thermodynamics as this would indicate a decrease in entropy due to heat dissipation.

Hence, the temperature in HHE must be interpreted as a nonequilibrium temperature. Several nonequilibrium thermodynamics theories have been proposed which would give the entropy generation a positive value when applying HHE. The basic argument is that if HHE is a correct physical model, one must modify the definition of entropy or internal energy of classical thermodynamics to justify HHE within a modified thermodynamics [22]. These so-called nonequilibrium thermodynamics propose that entropy is dependent on dissipative fluxes such as the heat flux, in addition to the classical thermodynamic variables. The most widely known nonequilibrium thermodynamics that justifies HHE is called extended irreversible thermodynamics (EIT) by Jou et al. [23]. It should be noted that the original irreversible thermodynamics proposed by Onsager [24] dealt with coupled transport phenomena such as thermoelectricity and is an extension of Fourier's law. Onsager explained that his theory

is not meant to be applied at time scales smaller than the relaxation time. The purpose of EIT is to extend macroscopic thermodynamics to non-local-equilibrium situations. EIT introduces dissipative fluxes as independent variables in addition to the classical thermodynamic variables to describe a system on time scales when these terms have not decayed, but that a sufficient amount of time has elapsed to allow the system to be described by only the dissipative fluxes and the classical thermodynamic variables. Jou and coworkers derived an equation for a generalized Gibbs equation and an expression for the entropy generation [22]. They further assumed that the non-local-equilibrium entropy generation must be positive. This assumption is used to limit the values that the dissipative fluxes can assume in order to meet the requirements of the second law under EIT. The mathematical details are not covered here, but a thorough overview of EIT can be found in the literature [22]. The only justification for EIT as a valid description of any real processes seems to be HHE, while at the same time the only theoretical justification for HHE seems to be EIT. Hence, EIT cannot be justified until HHE has been verified experimentally. A few papers contain experimental evidence of HHE and have been well cited by others as validation of HHE. Although these experiments have been questioned by many others, a critical examination is given later to complete this chapter.

3.5 Confusion With Other Physical Phenomena

Earlier pioneers like Cattaneo, Vernotte, and Taverneir did not examine the validity of HHE. When the thermal wave phenomenon was actually observed at lower temperatures, many believed that Cattaneo's equation should be a generalized Fourier's law [3]. It is important to differentiate between HHE and similar equations that have

physical foundations such as the two-temperature model (TTM) for ultrafast laser heating and the thermal wave phenomenon at low temperatures. TTM unlike HHE may depict certain physical phenomena that arise from coupling due to the interactions of electrons and phonons. The assumption is made that phonons are in equilibrium with phonons and that electrons are in equilibrium electrons, but the two types of particles are not in equilibrium with each other [9]. Thus, TTM gives two parabolic differential equations that are coupled with each other, and both equations are consistent with Fourier's law. Results corresponding to the prediction of TTM have been obtained experimentally for femtosecond pulsed-laser interaction with metals [25]. Furthermore, TTM does not predict any wavelike features nor does it predict a finite speed of propagation of a thermal signal.

Low-temperature behavior of thermal waves in liquid helium and a few dielectrics is fundamentally different from HHE, although both predict the second sound (or thermal wave velocity as described in Eq. (2.13). This behavior is actually due to two different scattering mechanisms for phonons, one associated with a normal process in which momentum is conserved and an Umklapp process in which the momentum is not conserved. Guyer and Krumhansl [26] derived the dispersion relation for second sound in solids based on BTE, where the collision contribution is approximated by two terms. The first term is given as

$$-\frac{f - f_{\lambda}}{\tau_{\mathrm{N}}} \tag{3.10}$$

which is associated with the normal scattering process. Since phonon momentum is conserved, the normal process will not change the direction of energy flow but it can change the distribution function. The change of the distribution function due to the

normal process will be zero when the distribution function is the same as that of a uniformly drifting phonon gas f_λ. The second collision term represents the Umklapp process and is given as

$$-\frac{f-f_0}{\tau_0} \tag{3.11}$$

The Umklapp scattering process does not conserve momentum and will eventually return the distribution function to the equilibrium distribution function f_0. The two relaxation times are the relaxation times associated with each of the scattering processes. Combining the scattering effects gives a simplified BTE for phonon scattering

$$\frac{\partial f}{\partial t}+\mathbf{v}\cdot\nabla f=-\frac{f-f_\lambda}{\tau_\mathrm{N}}-\frac{f-f_0}{\tau_0} \tag{3.12}$$

The solution of this linearized BTE gives the following differential equation for the effective temperature of phonons [27]:

$$\nabla^2 T+\frac{9\tau_\mathrm{N}}{5}\frac{\partial}{\partial t}\nabla^2 T=\frac{3}{\tau_0 v_\mathrm{a}^2}\frac{\partial T}{\partial t}+\frac{3}{v_\mathrm{a}^2}\frac{\partial^2 T}{\partial t^2} \tag{3.13}$$

where v_a is the average phonon speed. When the condition $\tau_\mathrm{N} << \tau_0$ is satisfied, the energy transfer is dominated by wave propagation. At higher temperatures, the scattering rate for the *U* processes is usually very high, and the *N* processes contribute little to the heat conduction or thermal resistance. Therefore, the reason why temperature waves have never been observed in dielectric crystals above 100 K is not because of their small relaxation time, in the range from 10^{-10} to 10^{-13} s, but because of the lack of mechanisms required for a second sound to occur. No experiments have ever shown a second sound in metals, as suggested by HHE. Note that Eq. (3.13) predicts a wavelike feature with a diffusion tail that is subject to the same criticism of infinite speed or propagation. A very

illustrative summary of solutions to the various heat conduction models was given by Tang and Araki [28]. Only the pure HHE has a finite speed of propagation; however, it is contradictory to statistical mechanics and violates the laws of thermodynamics as discussed earlier.

3.6 Misinterpretation of Experiments

Kaminski [29] performed experiments with several nonhomogenous materials (one of which was sand). Placed in the sand were an electric heating wire surrounded by electric insulation inside of a needle and a thermocouple inside of another needle used to measure the temperature. The experimental setup involved a thermocouple placed 6.8 mm and 16.8 mm from a restive heating source and found that heat propagated in sand at a velocity of 0.143 mm/s and τ_q for sand to be approximately 20 s. The value for relaxation time and velocity were determined when the penetration depth of the heat source reached the thermocouple. The penetration depth of a heat source is defined as the distance inside of the medium at which the temperature change has reached a certain threshold. This value of τ_q seems artificially high with regard to HHE and has no physical meaning as it is too large to represent an average time between scattering of particles. It is also possible that the solution that Kaminski obtained from Fourier's law was incorrect due to improper formulation of the problem or some other phenomena associated with a porous media such as sand grains. It should be noted that, although Fourier's law predicts the effect of a heat flux to be instantaneously felt everywhere throughout the medium, an effective propagation speed of heat can be defined base on the penetration depth. Even under Fourier's law this effective propagation speed can be very

slow as the effect at large distances will be negligible (below the sensitivity of the measurement instrument) until a sufficient amount of time has passed. Even though in theory the temperature will change a finite amount at large distances, the change will not be detectable by experimental means. Hence, the velocity that Kaminski observed may simply be an effective velocity of heat predicted by Fourier's law.

To demonstrate just how slow a diffusion process is, let us take for instance a semi-infinite slab with constant surface heat flux q_s'' . This problem has been solved in Carslaw and Jaeger [30], and the temperature distribution is given as

$$T(x,t) - T_i = \Delta T = 2q_s'' \frac{\sqrt{\alpha t}}{k}\left(\frac{\exp\left(-\zeta^2\right)}{\sqrt{\pi}} - \zeta \operatorname{erfc}(\zeta) \right) \tag{3.14}$$

where $\zeta = x/\sqrt{4\alpha t}$ is a similarity parameter and T_i is the initial temperature of the medium. The effective penetration depth can be defined based on a minimum temperature change in the medium. The diffusion velocity can be found by dividing the effective penetration depth by the elapsed time. The effective diffusion speed is shown in Fig. 3.2 for a semi-infinite medium with the thermal properties of (a) fused silica, (b) hardboard siding, and (c) copper respectively at 300 K [31]. Three curves show three different temperature change thresholds used to define the effective penetration depth. At a distance of 20 mm inside of the medium the effective thermal velocity for a temperature rise of ΔT = 1 mK will result in an effective thermal velocity of about 1.67 mm/s for fused silica, 0.31 mm/s for hardboard siding, and 122 mm/s for copper. The effective velocity of a diffusion process may vary with the geometry, position, heat flux, minimum temperature rise, and properties of a material. Nevertheless, it can be seen that the diffusion process results in very slow thermal signal propagation, contrary to the

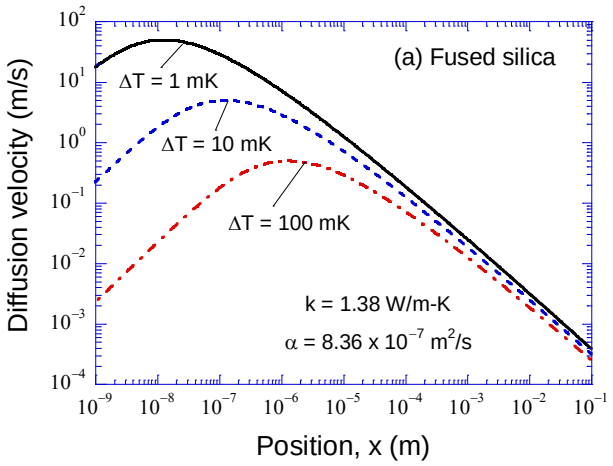

a) Fused Silica

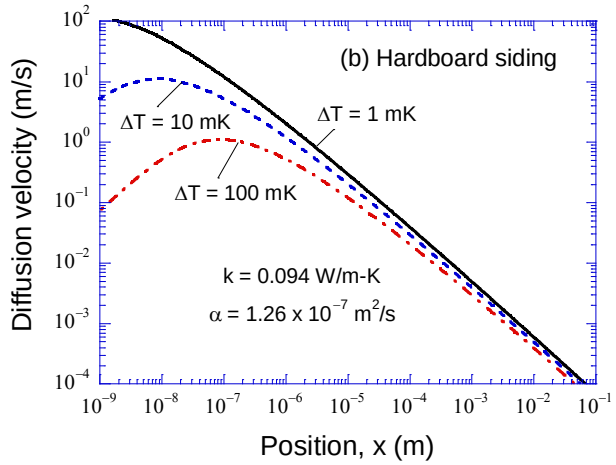

b) Hardboard Siding

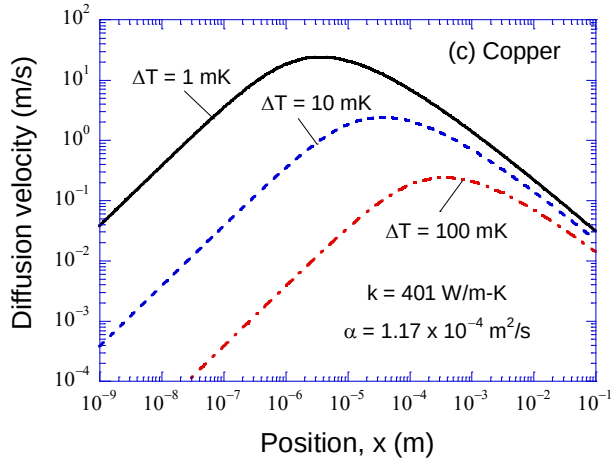

c) Copper

Figure 3.2: Velocity of diffusion for a semi-infinity medium with constant surface flux of $q''_s = 2\times10^5$ W/m^2: (a) Fused Silica; (b) hardboard siding; (c) copper. The thermophysical properties of these materials are taken from [26]

belief of many researchers. As early as 1997, Tzou [6] pointed out that the thermal wave model is unsuitable for describing transient thermal behavior in casting sand (or other nonhomogeneous materials). However, many recent publications on heat transfer in biological systems continue to misinterpret the speed of diffusion as the speed of temperature waves in HHE.

Mitra et al. [32] performed an experiment on processed meat to show that temperature waves have a finite propagation speed in certain biological media and other materials with nonhomogenous inner structures. Two samples held at different initial temperatures of identical processed meat were brought into contact and the temperature was measured by a thermocouple embedded in each of the samples. The experimental results showed a temperature jump after a finite amount of time had passed rather than a smooth transition such as would be predicted by Fourier's law. In addition, two other experiments were performed to demonstrate phenomena associated with temperature waves such as superposition of two temperature waves and one additional experiment intending to demonstrate the finite propagation speed of temperature waves in a medium. In one of their experiments, a slab (14.3°C) was sandwiched between a large cold sample (6.2°C) and a large hot sample (24.1°C). Results shown in the paper indicated a superposition phenomenon of the temperature waves as measured by a thermocouple embedded in the thin meat sample. If the temperature of HHE is an effective nonequilibrium temperature, it seems unlikely one would be able to measure this temperature with a simple thermocouple. Their results were never repeated by themselves or verified by others.

A similar experiment was performed by Herwig and Beckert [33] who used water flowing through a copper pipe in a box filled with a desired medium. The experiment was conducted with both sand and processed meat similar to the experiments used to validate HHE [29, 32]. The results obtained in Ref. [33] showed that the temperature distribution predicted by Fourier's law was within the uncertainty of the temperature values obtained in their experiment.

If the experimental results validating HHE were reliable, then there would be a plethora of similar findings in the literature; such results however are lacking. It seems unlikely that nonporous media would sometimes obey HHE and sometimes obey PHE at such relatively long time scales as in the aforementioned experiments. On a microscopic basis, diffusion-like behavior would be expected and any disagreement may be due to other phenomena associated with the nonhomogeneous inner structure not related to HHE. At the present time, conclusive experimental results supporting HHE do not exist.

Finally, it should be reminded that the experimental results showing thermal waves in liquid helium and cryogenic dielectric crystals are not a result of HHE, but are rather due to another phenomenon. This phenomenon is only observable at low temperatures where the normal process of phonon scattering becomes more significant. This gives rise to two relaxation mechanisms for phonon scattering, one associated with the normal process and one with the Umklapp process, leading to a two-relaxation time model. This model is only valid when the time scale is greater than the relaxation time of the normal process and less than the combined relaxation time of both processes [9].

CHAPTER 4

PHONON RADIATIVE ENTROPY GENERATION

Despite numerous studies on the phonon radiative transfer, there seems to be a lack of research dealing with the entropy generation associated with phonon radiation. Entropy generation associated with heat conduction is well known [34]. However, the conventional control volume analysis is for large scales when diffusion is the dominant process of heat conduction. Entropy of radiation has been used to derive Planck's law of thermal radiation and can model the entropy generation in radiative transfer both at the boundaries as well as in participating medium [35-39]. Furthermore, an understanding of the entropy transfer and generation processes in phonon radiation can deepen the knowledge of irreversibility associated with lattice conduction from small to large scales.

This chapter describes a study on the entropy of phonon radiation to provide new insight into the phonon heat conduction process. The 1D phonon radiative transport between two constant-temperature thermal reservoirs (black walls) at steady state, as illustrated in Fig. 2.1, is considered to develop fundamental arguments that could be extended to multiple dimensions. The boundaries or surfaces of the medium are treated as infinite thermal reservoirs and are referred to throughout this chapter as walls due to the arbitrary choice of vertical orientation. It extends the analogy between photons and phonons to understand the process of entropy generation at all length scales. A phonon brightness temperature is defined that is frequency and direction dependent.

4.1 Radiative Equilibrium and Local Equilibrium

The radiative equilibrium is the condition at which [40, 41]

$$\nabla \cdot \mathbf{q}'' = 0 \tag{4.1}$$

which corresponds to the case where there are no sources or sinks in the medium. In the case of steady-state conduction, Eq. (4.1) holds for phonon transport. For the 1D case, it implies that

$$\frac{\partial q_x''}{\partial x} = 2\pi \int_0^\infty \int_{-1}^1 \mu \frac{\partial I_\omega(\omega, \mu)}{\partial x} d\mu d\omega = 0 \tag{4.2}$$

Integrating Eq. (2.19) over the frequency and direction cosine and applying Eq. (4.2), one obtains the following relation:

$$2\int_0^\infty \frac{I_\omega^0}{\Lambda} d\omega = \int_0^\infty \int_{-1}^1 \frac{I_\omega}{\Lambda} d\mu d\omega \tag{4.3}$$

while Eq. (4.1) is applicable to steady state only, it was shown that Eq. (4.3) is also applicable to transient EPRT [14]. For a gray medium, the equilibrium condition reduces to

$$\int_0^{\omega_D} I_\omega^0 d\omega = \frac{1}{2} \int_0^{\omega_D} \int_{-1}^1 I_\omega d\mu d\omega \tag{4.4}$$

where the upper limit is replaced by the Debye cut-off frequency ω_D, which is related to the Debye temperature by $\Theta_D = \hbar\omega_D / k_B$ [9, 12]. Furthermore, when the temperature of the medium is much lower than the Θ_D, the total equilibrium intensity can be expressed as

$$I^0(T) = \int_0^{\omega_D} I_\omega^0 d\omega \approx \frac{\sigma_{SB}' T^4}{\pi} \tag{4.5}$$

where $\sigma'_{\mathrm{SB}} = \dfrac{\pi^2 k_{\mathrm{B}}^4}{40\hbar^3 v_{\mathrm{a}}^2}$ may be thought as the Stefan-Boltzmann constant for phonons [9, 42]. Using the total intensity defined as $I = \int_0^{\omega_{\mathrm{D}}} I_\omega d\omega$, Eq. (4.4) can be simplified to the following:

$$I^0 = \frac{1}{2}\int_{-1}^{1} I d\mu \tag{4.6}$$

Hence, for a gray medium, one can integrate Eq. (2.19) over all frequencies and substitute Eq. (4.6) for $I^0(T^*)$ to obtain

$$\mu \frac{\partial I}{\partial x} = \frac{1}{\Lambda}\left(\frac{1}{2}\int_{-1}^{1} I d\mu - I\right) \tag{4.7}$$

When the boundary conditions are prescribed, Eq. (4.7) can be solved for *I* using standard techniques in radiative transfer, such as the discrete ordinates method and the Monte Carlo method [40, 41]. The effective temperature $T^*(x)$ throughout the medium can be determined using Eq. (4.5). Once the temperature distribution is known, the intensity can be divided into right and left hemispheres. For black walls, the local intensity can be expressed as follows [9]:

$$\begin{aligned} I_\omega^+(x,\omega,\mu) &= I_\omega^0(\omega,T_1)\exp\left(-\frac{x}{\Lambda\mu}\right) \\ &\quad + \int_0^x I_\omega^0\left(\omega,T^*(\xi)\right)\exp\left(-\frac{x-\xi}{\Lambda\mu}\right)\frac{d\xi}{\Lambda\mu}, \quad \text{for } \mu > 0 \end{aligned} \tag{4.8}$$

$$\begin{aligned} I_\omega^-(x,\omega,\mu) &= I_\omega^0(\omega,T_2)\exp\left(\frac{L-x}{\Lambda\mu}\right) \\ &\quad - \int_x^L I_\omega^0\left(\omega,T^*(\xi)\right)\exp\left(\frac{x-\xi}{\Lambda\mu}\right)\frac{d\xi}{\Lambda\mu}, \quad \text{for } \mu < 0 \end{aligned} \tag{4.9}$$

which can be evaluated using numerical integration to obtain the local phonon intensity in any direction and at any frequency.

In some studies [7, 14], a more restrictive assumption was used such that phonon radiative equilibrium exists at every frequency so that

$$I_\omega^0 = \frac{1}{2}\int_{-1}^{1} I_\omega d\mu \tag{4.10}$$

which is equivalent to say that

$$\frac{\partial q''_\omega}{\partial x} = 2\pi\int_{-1}^{1} \mu \frac{\partial I_\omega(\omega,\mu)}{\partial x} d\mu = 0 \tag{4.11}$$

From the derivation in the preceding section, Eqs. (4.10) and (4.11) are not needed in order to solve EPRT. As a matter of fact, even for a gray medium, Eqs. (4.10) and (4.11) are not satisfied unless the medium is acoustically thick. It was pointed out by Zhang [9] that Eq. (4.11) is equivalent to the local equilibrium assumption but without a proof. In the following, the local equilibrium conditions are discussed and shown to be consistent with Eq. (4.10) or (4.11).

Under the relaxation time approximation, the local equilibrium assumption states that

$$\frac{\partial f}{\partial x} = \frac{\partial f_0}{\partial x} \quad \text{or} \quad \frac{\partial I_\omega}{\partial x} = \frac{\partial I_\omega^0}{\partial x} \tag{4.12}$$

To the first order approximation, the intensity can be expressed as follows [12, 40]:

$$I_\omega \approx I_\omega^0 - \mu\Lambda \frac{\partial I_\omega^0}{\partial T}\frac{\partial T}{\partial x} \tag{4.13}$$

where T is used instead of T^* to signify local equilibrium has been established. For Eq. (4.13) to be a good approximation, the implicit assumptions are $Kn \ll 1$, i.e., the medium is acoustically thick, and in addition

$$\frac{\partial T}{\partial x} << \frac{T}{\Lambda} \tag{4.14}$$

Equation (4.14) requires that the temperature of the medium should not change abruptly over a mean free path (Λ). Under the assumptions given in Eqs. (4.13) and (4.14), the Fourier law at steady state can be derived such that

$$q_x'' = -k\frac{dT}{dx} = -\frac{dT}{dx}\int_0^\infty \frac{4\pi}{3}\Lambda\frac{\partial I_\omega^0}{\partial T}d\omega \tag{4.15}$$

where *k*, given by the frequency integral, is the thermal conductivity. It should be noted that the assertion that the hyperbolic heat equation can be derived from BTE or EPRT, by keeping the transient term in Eq. (2.14), is misleading due to the fact that Eq. (4.14) is rarely satisfied at time scales shorter than the relaxation time. As pointed out the previous chapter and in the literature recently [43], Cattaneo's equation was misconceived and does not extend the applicable regime of Fourier's law as often thought in the heat transfer community.

If both sides of Eq. (4.13) are integrated over the direction cosine, the result will be the same as Eq. (4.10), suggesting that local equilibrium is a sufficient condition of Eq. (4.10). Furthermore, from Eqs. (4.8) and (4.9), the spatial derivative of the spectral heat flux can be expressed as [9],

$$\begin{aligned}\frac{\partial q_\omega''}{\partial x} = {} & \frac{4\pi}{\Lambda}I_\omega^0\left(\omega,T^*(x)\right) - \frac{2\pi}{\Lambda}\int_0^L I_\omega^0\left(\omega,T^*(\xi)\right)E_1\left(\frac{|x-\xi|}{\Lambda}\right)\frac{d\xi}{\Lambda} \\ & - \frac{2\pi}{\Lambda}I_\omega^0\left(\omega,T_1\right)E_2\left(\frac{x}{\Lambda}\right) - \frac{2\pi}{\Lambda}I_\omega^0\left(\omega,T_2\right)E_2\left(\frac{L-x}{\Lambda}\right)\end{aligned} \tag{4.16}$$

where $E_m(x) = \int_0^1 \mu^{m-2}e^{-x/\mu}d\mu$ is the *m*th exponential integral. The last two terms on the right-hand side of Eq. (4.16) originated from the wall emission. It can be seen that, in

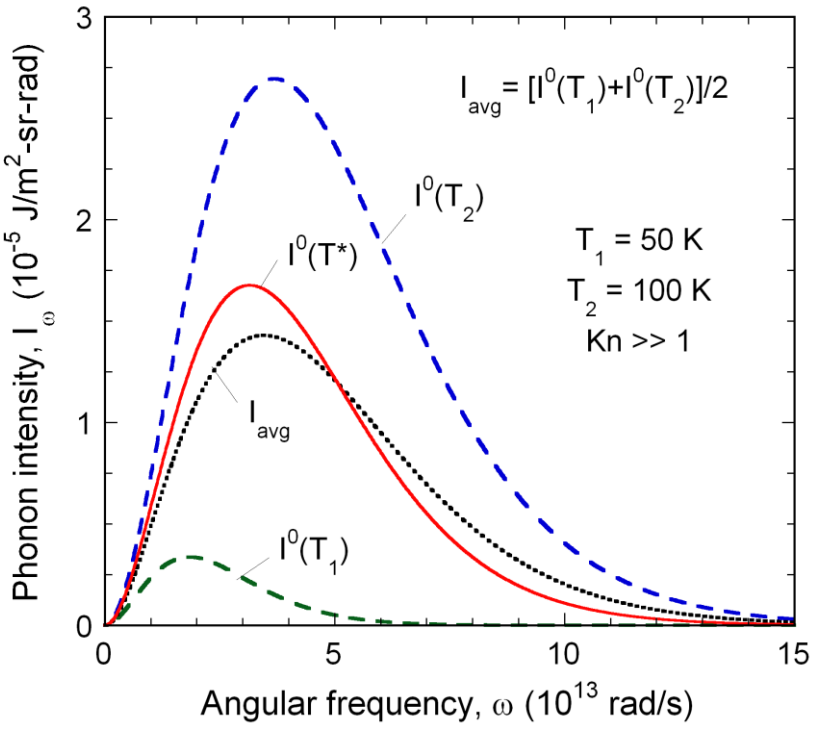

Fig. 4.1 Phonon intensity at different frequencies corresponding to two black walls at temperatures $T_1 = 50\,\mathrm{K}$ and $T_2 = 100\,\mathrm{K}$. The equilibrium temperature of the medium is denoted by T^* and I_{avg} is the average intensity of the two wall distributions.

general, $\partial q''_\omega / \partial x \neq 0$ unless $L >> \Lambda$ and x is not too close to the wall, i.e., in the acoustically thick limit. Therefore, Eq. (4.10) or (4.11) can be viewed as the local equilibrium condition that should not be imposed in solving EPRT for thin films.

Consider a thin film in Casimir's limit where ballistic phonon transport dominates between two black walls. One may view phonon radiation as being emitted from two black walls with no scattering and little absorption/emission inside of the medium. Figure 4.1 shows the equilibrium intensity distributions evaluated at the wall temperatures, along with the exact equilibrium intensity distribution $I^0_\omega(\omega, T^*)$ evaluated using the effective temperature of the medium at $x = L/2$. The average speed of sound is taken as that of

diamond, i.e., $v_a = 12288$ m/s [7]. The intensity integration over the direction cosine is the same as the algebraic average $I_{avg}(\omega)$ of the intensities of the two walls. The two curves do not overlap except at a single finite frequency. In general, $I^0_\omega(T^*) > I_{avg}$ at lower frequencies and $I^0_\omega(T^*) < I_{avg}$ at higher frequencies. If $I_{avg}(\omega)$ were taken as the equilibrium distribution, according to Eq. (4.10), a frequency-dependent effective temperature would be obtained. It is worth noting that the results presented in Refs. [7, 14] are correct, disregards the excessive assumption in the form of Eq. (4.10) made in the analysis of these studies.

4.2 Classical Entropy of Diffusion

In EPRT, the phonon radiation process is analogous to photon radiation with absorption and emission, but without scattering, as prescribed by Eq. (2.19). As suggested by Prasher [44], a phonon scattering phase function may be introduced to derive a more general EPRT that includes the in-scattering term just like the conventional ERT for thermal radiation. This would require some modification of the collision term on the right-hand side of Eq. (2.14). For simplicity, the in-scattering term is excluded in the present study.

When comparing photon and phonon radiation, it is important to keep in mind the physical differences between the two processes. In thermal radiation in a participating medium, the medium or gas itself emits radiation at its local (equilibrium) temperature. For phonon radiation, the scattering term remains after simplification of the collision term in the BTE and is manifested by the emission and absorption terms in EPRT due to

the assumption of linearity. Despite the differences, it is convenient to think of phonon radiation as also having a local medium, which emits phonons according to the equilibrium distribution at the effective temperature (T^*). Under the relaxation time approximation, the distribution function is not too far from equilibrium and the medium temperature is thus obtained by the equilibrium intensity (I^0). Furthermore, such a medium can also absorb phonon radiation. While the total emitted and absorbed energy must be the same, as required by the radiative equilibrium condition, the absorbed and emitted energy at any particular frequency are in general not equal to each other, unless Eq. (4.10) is satisfied. One should keep in mind that in actuality all phonons are governed by the nonequilibrium distribution function (*f*) or intensity (I_ω) that is determined by solving the BTE or EPRT.

The process of entropy generation due to phonon transport is caused largely by the redistribution of the phonon radiative intensity over the spectrum. If a medium lies at constant temperature (no heat transfer), then phonon transport still takes place but the phonon "emission" and "absorption" both correspond to equilibrium distributions at the corresponding temperature of the medium in any location. This of course results in no net transfer of energy in any direction and, therefore, no entropy generation since the phonon intensity cannot be redistributed across the spectrum. If there is a temperature gradient in the medium (i.e., temperature difference between the two walls), the contribution of phonon emission from one side will have a different intensity distribution than the other. Since the intensity of phonon emission decays rapidly within a few mean free paths, the majority of frequency redistribution occurs within a few mean free paths where the temperature difference is generally small for a thick medium. However, small differences

in intensity at each frequency can result in relatively large heat transfer and entropy generation when taking into account the large frequency range of phonons. Temperature gradients result in a gradual spectral shift of the phonon intensity, towards longer wavelengths in the direction of decreasing temperature, across the medium.

The entropy of thermal radiation has been extensively studied [35-39]. It is convenient in the analysis of radiative entropy generation to introduce a frequency dependent temperature, known as the brightness temperature, and an entropy intensity which is analogous to radiation intensity but in terms of the flow of entropy instead of energy. The brightness temperature can be thought of as a measure of temperature of the nonequilibrium distribution of phonon radiation in a given direction at a given frequency. The brightness temperature is the temperature of an equilibrium distribution which has the same intensity as the nonequilibrium distribution at a given frequency. The inverse of the brightness temperature can be found by [9],

$$\frac{1}{T_\omega(\omega,\theta)} = \frac{k_\mathrm{B}}{\hbar\omega}\ln\left(1+\frac{\beta\hbar}{8\pi^3 v_\mathrm{a}^2 I_\omega}\right) \tag{4.17}$$

where β depends on the number of phonon modes but is taken to be 3 (two transverse and one lateral mode) in the present study. The entropy intensity is defined based on the phonon radiation intensity as [9, 39],

$$L_\omega = \frac{\beta k_\mathrm{B}\omega^2}{8\pi^3 v_\mathrm{a}^2}\left[\left(1+\frac{8\pi^3 v_\mathrm{a}^2 I_\omega}{\beta\hbar\omega^3}\right)\ln\left(1+\frac{8\pi^3 v_\mathrm{a}^2 I_\omega}{\beta\hbar\omega^3}\right)-\frac{8\pi^3 v_\mathrm{a}^2 I_\omega}{\beta\hbar\omega^3}\ln\left(\frac{8\pi^3 v_\mathrm{a}^2 I_\omega}{\beta\hbar\omega^3}\right)\right] \tag{4.18}$$

Furthermore, the phonon entropy intensity and the brightness temperature are related by the definition of thermodynamic temperature as follows:

$$\frac{1}{T_\omega(\omega,\theta)} = \frac{\partial L_\omega}{\partial I_\omega}\Bigg)_\omega \tag{4.19}$$

The 1D entropy generation rate per unit volume in radiation transfer in a participating medium is given by [38, 39],

$$s'''_{\text{gen}} = 2\pi \int_0^{\infty} \int_{-1}^{1} \frac{I_\omega^0 - I_\omega}{\Lambda} \left(\frac{1}{T_\omega} - \frac{1}{T^*} \right) d\mu d\omega \tag{4.20}$$

Equation (4.20) can be used to evaluate the entropy generation in the medium for phonon radiation. Due to the temperature jump at the boundaries, there will also be entropy generation at the wall, which can be written as [9, 38, 39]

$$s''_{\text{gen,w}} = 2\pi \int_0^{\omega_{\text{D}}} \int_0^{1} \left[\frac{I_{\text{in},\omega} - I_{\text{out},\omega}}{T_{\text{w}}} - \left(L_{\text{in},\omega} - L_{\text{out},\omega} \right) \right] \mu d\mu d\omega \tag{4.21}$$

where T_{w} is the wall temperature, and for the right wall noting that μ should be replaced by $-\mu$ to make it positive. The term with $\mu\left(I_{\text{in},\omega} - I_{\text{out},\omega}\right)/T_{\text{W}}$ is net heat flux from the medium to the wall by phonon radiation over the temperature and the term with $\mu\left(L_{\text{in},\omega} - L_{\text{out},\omega}\right)$ is the net entropy flux from the medium to the wall. Note that the entropy generation inside of the wall in a real system may depend on the acoustical properties of the boundaries and may not be well described by a black wall model. In the present study, only the entropy generations between the walls and the medium and inside the medium are considered since each wall is assumed to be at a uniform temperature (i.e., as a thermal reservoir).

Under the local equilibrium assumption, $T^*(x)$ in Eq. (4.20) can be replaced by $T(x)$, and one can use the first-order expansion to approximate T_ω in the following,

$$T_\omega(I_\omega) \approx T\left(I_\omega^0\right) + \left.\frac{\partial T}{\partial I_\omega}\right|_{I_\omega^0} \left(I_\omega - I_\omega^0\right) \tag{4.22}$$

From Eqs. (2.18) and (4.22), it can be seen that

$$\left.\frac{\partial T}{\partial I_\omega}\right|_{I_\omega^0} = \frac{\partial T}{\partial I_\omega^0} \tag{4.23}$$

Substituting Eqs. (4.13), (4.22), and (4.23) into Eq. (4.20) and simplify using Eq. (4.14), one obtains

$$s'''_{\text{gen}} = -\left(\frac{1}{T}\frac{dT}{dx}\right)^2 \int_0^\infty \Lambda \frac{4\pi}{3}\frac{dI_\omega^0}{dx} d\omega \tag{4.24}$$

Compared with Eq. (4.15) for the heat flux in the diffusion limit, Eq. (4.24) can be expressed as

$$s'''_{\text{gen}} = \frac{q''_x \nabla T}{T^2} \tag{4.25}$$

which is the classical expression of entropy generation during heat diffusion [34] as well as thermal radiation in the optically thick limit [45].

Equations (4.20) and (4.21) are general case of entropy generation and can be evaluated after the EPRT solution is obtained. The total entropy generation inside of the medium under the radiation model can be found by adding the wall entropy generation and the generation inside of the medium. Under the local equilibrium assumption, the entropy generation due to phonon radiation can be approximated with the entropy generation model derived based on heat diffusion from control volume analysis. Liu and Chu [46] studied entropy generation using numerical techniques to solve the radiative transfer equation and showed that a medium must be optically thick for the diffusion model correctly predict the entropy generation.

4.3 Numerical Study of Phonon Radiative Entropy

The techniques for solving the radiative transfer equation in a participating medium are numerous [40, 41]. In the present study, the discrete ordinates method is employed except when the *Kn* is very small. For a 1D thin medium a solution with 16 discrete directions is used with weights and abscissas corresponding to the standard Gaussian quadrature technique. The temperature solution is obtained directly using linear algebra techniques to get an exact solution to the system of equations. For $Kn \leq 0.001$, the discrete ordinates method becomes very inefficient and time consuming to obtain converging solutions. A diffusion approximation [47] is used to solve the temperature distribution inside of the medium, coupled with the jump boundary condition at the walls, in order to satisfy the condition of a continuous heat flux at the wall and throughout the medium. The jump boundary condition can be expressed as [40, 47].

$$\pi I^0(T_1) - \pi I^0\left(T^*(0)\right) = \left(\frac{1}{\varepsilon_1} - \frac{1}{2}\right) q_x'' \tag{4.26}$$

$$\pi I^0\left(T^*(L)\right) - \pi I^0(T_2) = \left(\frac{1}{\varepsilon_2} - \frac{1}{2}\right) q_x'' \tag{4.27}$$

where ε_1 and ε_2 are the emissivities of the walls and both are equal to 1 (blackbody). Equations (4.26) and (4.27) can be iteratively solved with the Rosseland diffusion equation [40],

$$q_x'' = -\frac{16\Lambda}{3}\sigma_{\mathrm{SB}}' T^3 \frac{dT}{dx} \tag{4.28}$$

when *Kn* is extremely small. To the first order approximation, Eqs. (4.26) through (4.28) can also give a linear temperature distribution inside the medium with temperature jumps at the boundaries. The application of Eq. (4.28) implies that the thermal conductivity is

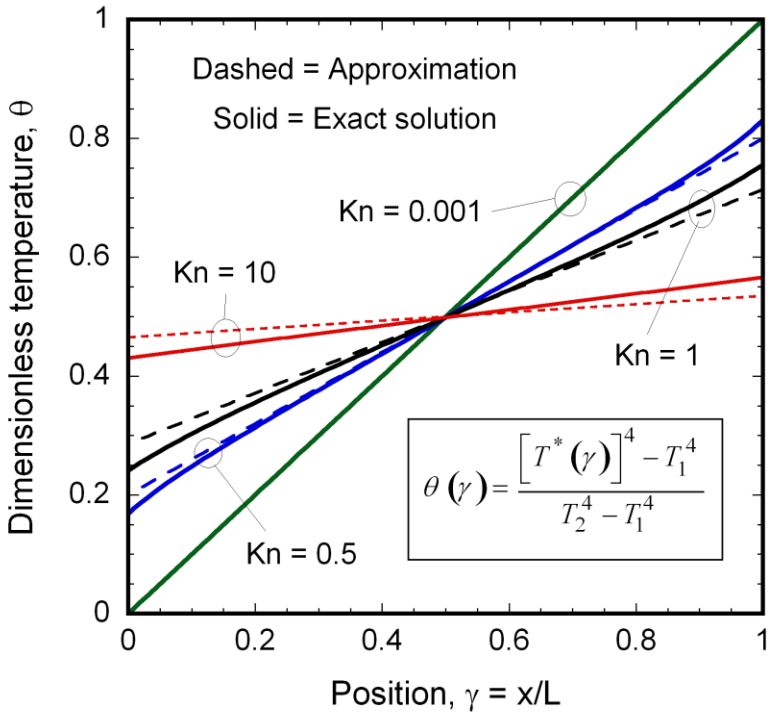

Fig. 4.2 Temperature distribution inside of medium between two black walls as given by the EPRT (solid) and the diffusion approximation (dashed) for various *Kn*.

fixed, that is proportional to T^3. This is reasonable since at low temperatures, phonon specific heat is proportional to T^3 and the scattering rate is governed by defect scattering that is independent of temperature.

Figure 4.2 shows several solutions for the effective temperature inside of a medium for different *Kn* plotted in terms of the dimensionless position $\gamma = x/L$. Solutions of the EPRT using the discrete ordinates method (exact) and compared with the diffusion approximation with temperature jump at the boundaries. When *Kn* = 0.001, the two methods give essentially the same results. As *Kn* increases, deviation becomes larger, suggesting that the diffusion approximation is no longer applicable.

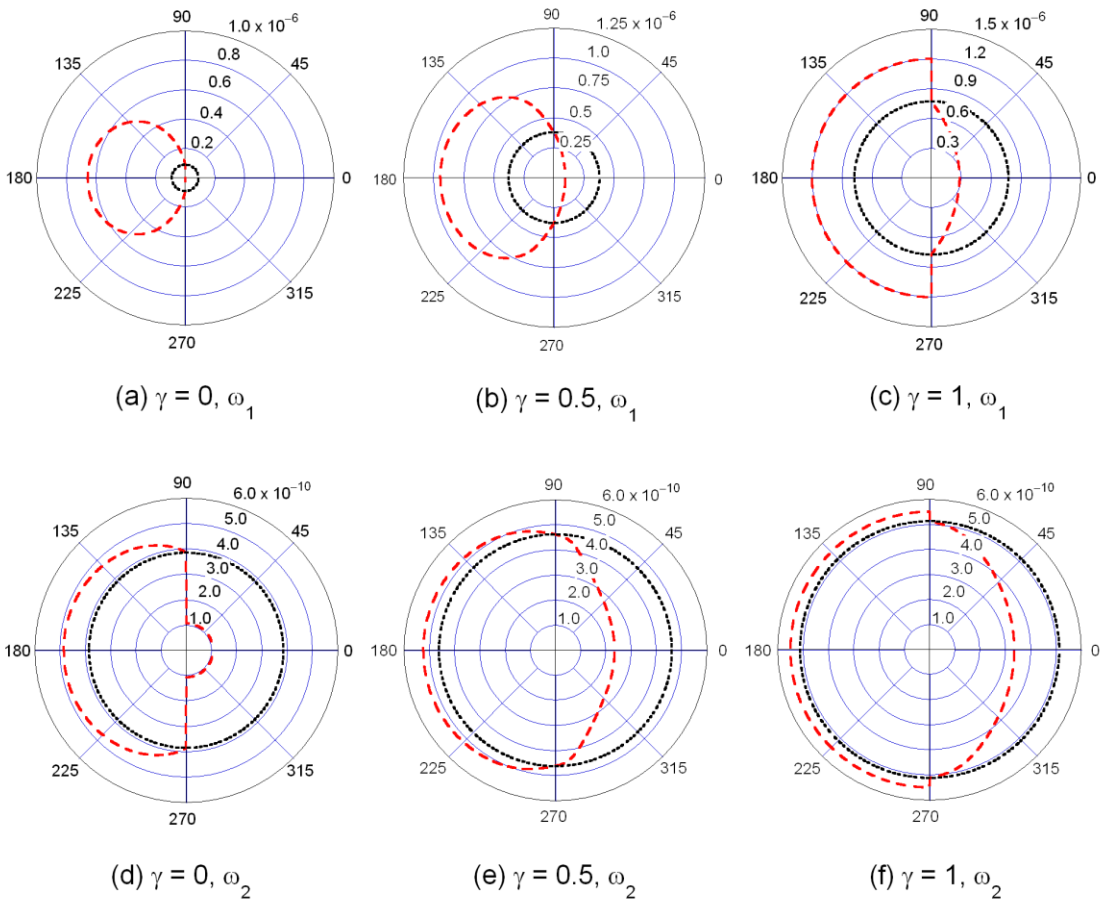

Fig. 4.3 Phonon intensity I_ω (red dashed) and $I_\omega^0(T^*)$ (black dotted) distributions inside a medium with *Kn* = 1 when $T_1 = 10\,\mathrm{K}$ and $T_2 = 50\,\mathrm{K}$, at three different locations and two different frequencies, i.e., $\omega_1 = 4\times10^{13}$ rad/s and $\omega_2 = 1\times10^{11}$ rad/s. The unit of intensity is $\mathrm{J/m^2\cdot sr\cdot rad}$.

The spectral intensity can be calculated for different *Kn* based on the exact solution. For diamond, the relaxation time is independent of temperature at low temperatures and the mean free path is calculated to be $\Lambda = 1.343\ \mu\mathrm{m}$ from Ref. [7]. The Debye temperature of diamond is 1860 K, which is much higher than the temperatures considered in the present study. The speed of sound is $v_\mathrm{a} = 12288$ m/s as mentioned before. These parameters are used to obtain all the numerical results in the present study.

The intensity distribution is shown in Fig. 4.3 for $Kn = 1$ with $T_1 = 10$ K and $T_2 = 50$ K, at three locations inside the medium and for two frequencies. Since the mean free path is equal to the film thickness, approximately 37% of the phonon radiation will be preserved from one wall to the other in the direction normal to the walls. The calculated temperatures in the medium are $T^*(\gamma = 0) = 36.6$ K, $T^*(\gamma = 0.5) = 42.1$ K, and $T^*(\gamma = 1) = 46.0$ K. There is a larger temperature jump near the lower temperature wall. The dotted circle represent the phonon equilibrium intensity (or emitted intensity), $I_\omega^0(T^*)$, which is isotropic and increases from the left to the right. It should be noted that the change of $I_\omega^0(T^*)$ is more prominent at higher frequencies than at lower frequencies. This is because the distribution function is more sensitive to temperature change at higher frequencies. The dashed curve is the actual intensity $I_\omega(\gamma)$, which is always larger in the left hemisphere than in the right hemisphere since $T_2 > T_1$ and heat transfer is from right to the left. Note that $I_\omega(\gamma = 0)$ for $\cos\theta > 0$ is the emitted intensity from the left wall and $I_\omega(\gamma = 1)$ for $\cos\theta < 0$ is the emitted intensity from the right wall. It is interesting to compare the area inside the $I_\omega(\gamma)$ and $I_\omega^0(T^*)$ curve. At high frequencies, $\int_{-1}^{1} I_\omega^0\left(T^*\right) d\mu < \int_{-1}^{1} I_\omega d\mu$ so the area surrounded by $I_\omega(\gamma)$ is bigger as can be seen from the upper three figures. At lower frequencies, the opposite is true as can be seen from the lower figures in Fig. 4.3. Clearly, Eq. (4.10) is not satisfied for $Kn = 1$ since the condition of local equilibrium is not met.

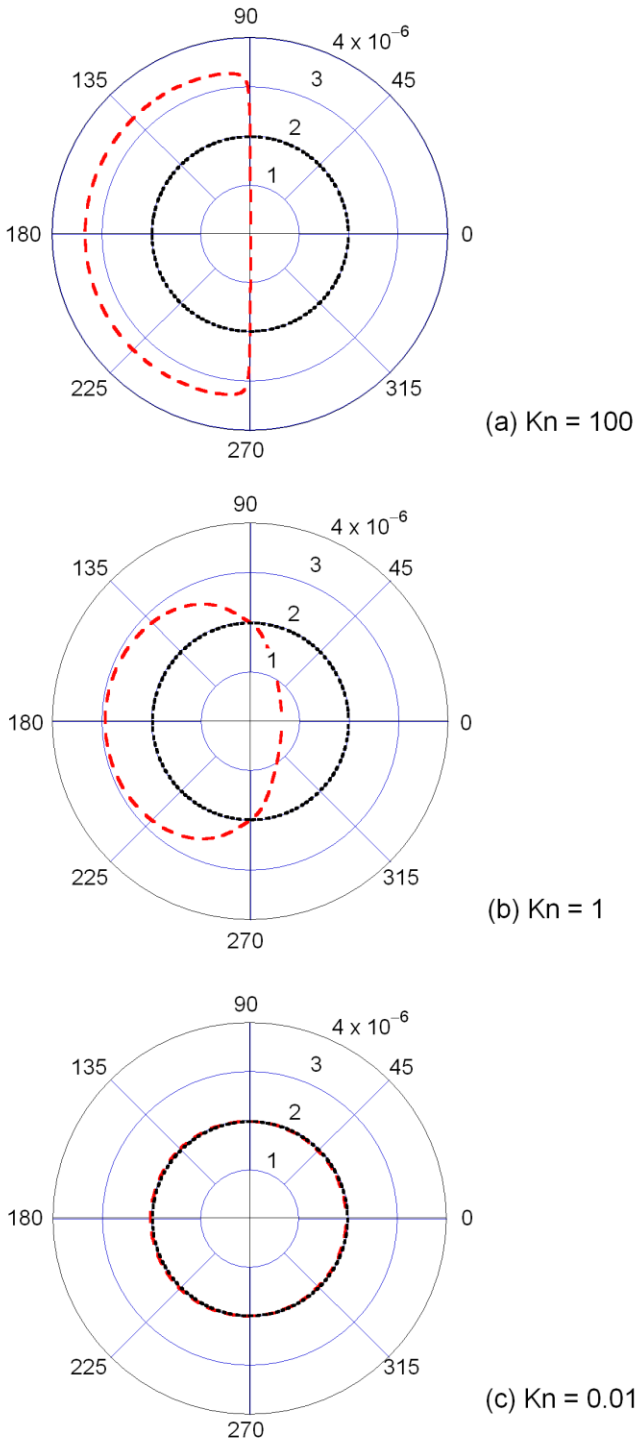

Fig. 4.4 Phonon intensity I_ω (red dashed) and $I_\omega^0(T^*)$ (black dotted) distributions at the center of the medium: (a) *Kn* = 100; (b) *Kn* = 1; (c) *Kn* = 0.01. The unit of intensity is $\mathrm{J/m^2 \cdot sr \cdot rad}$, the wall temperatures are $T_1 = 10\,\mathrm{K}$ and $T_2 = 50\,\mathrm{K}$, and the angular frequency is set to $\omega = 1.7 \times 10^{13}$ rad/s.

In Fig. 4.4, the intensity distribution at the center of the medium for different Kn is plotted at a single frequency for $T_1 = 10$ K and $T_2 = 50$ K. One may view the cases for different film thicknesses. As the thickness of the medium becomes larger, the nonequilibrium and equilibrium distributions appear to overlap in all directions. This suggests that the classical definition of temperature in heat conduction becomes reasonable in the diffusion limit. However, a small difference between the two distributions must always be present since $I_\omega(\gamma)$ must be anisotropic in order for the heat transfer to occur. Although the difference between $I_\omega(\gamma)$ and $I_\omega^0(T^*)$ may be very small at the same location, integration over all frequencies can still result in a significant amount of heat transfer in the diffusion limit. Both Figs. 4.3 and 4.4 show some properties unique to the 1D heat transfer problem. For instance, the symmetry over the horizontal line is due to the fact that the transport properties are independent of ϕ. At the same location and frequency, $I_\omega(180°)$ is always the largest and $I_\omega(0°)$ is always the smallest. One can think about the effective medium thickness according to $L/\cos\theta$. Hence, in the *x* direction, the effect of ballistic transport is the strongest. The curves of $I_\omega(\gamma)$ and $I_\omega^0(T^*)$ always cross over each other at $\theta = 90°$ or $\theta = 270°$ (i.e., when $\mu = 0$). In essence, the medium along the vertical direction is infinitely thick.

Figure 4.5 shows the brightness temperature at the center of the medium under the same conditions as in Fig. 4.4, except at two different frequencies. The two separate frequencies are considered to illustrate the difference in brightness temperature at high and low frequencies. From this figure it appears that the higher-frequency curve always bounds the lower-frequency curve for the same *Kn*. Furthermore, intensity in the

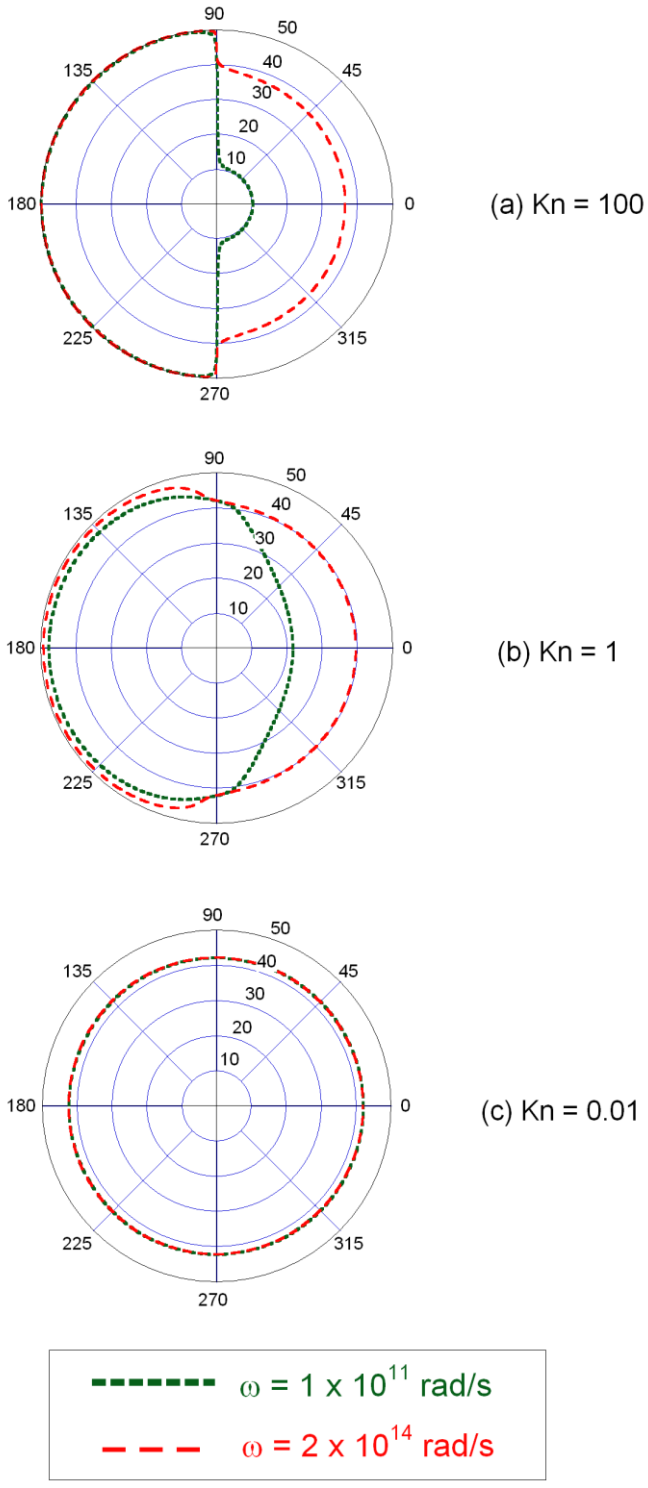

Fig. 4.5 Polar plots of the brightness temperature $T_\omega(\omega,\theta)$ at two frequencies, at the center of the medium, for (a) Kn = 100; (b) Kn = 1; (c) Kn = 0.01. The wall temperatures are $T_1 = 10\,\mathrm{K}$ and $T_2 = 50\,\mathrm{K}$.

direction $\theta = 0$ has the largest temperature variance at different frequencies. For smaller *Kn*, it becomes apparent that the brightness temperature will converge to the medium temperature at every frequency as shown in Fig. 4.5(c), where the curve looks like circles and overlap with each other at different frequencies. It should be emphasized that these curves cannot be perfect circles in order for heat transfer to occur.

Figure 4.6 plots the phonon brightness temperature as a function of frequency for $Kn = 1$ at the center of the medium, with several direction cosine values. The other parameters are the same as in Fig. 4.5. It can be seen that the results are consistent with

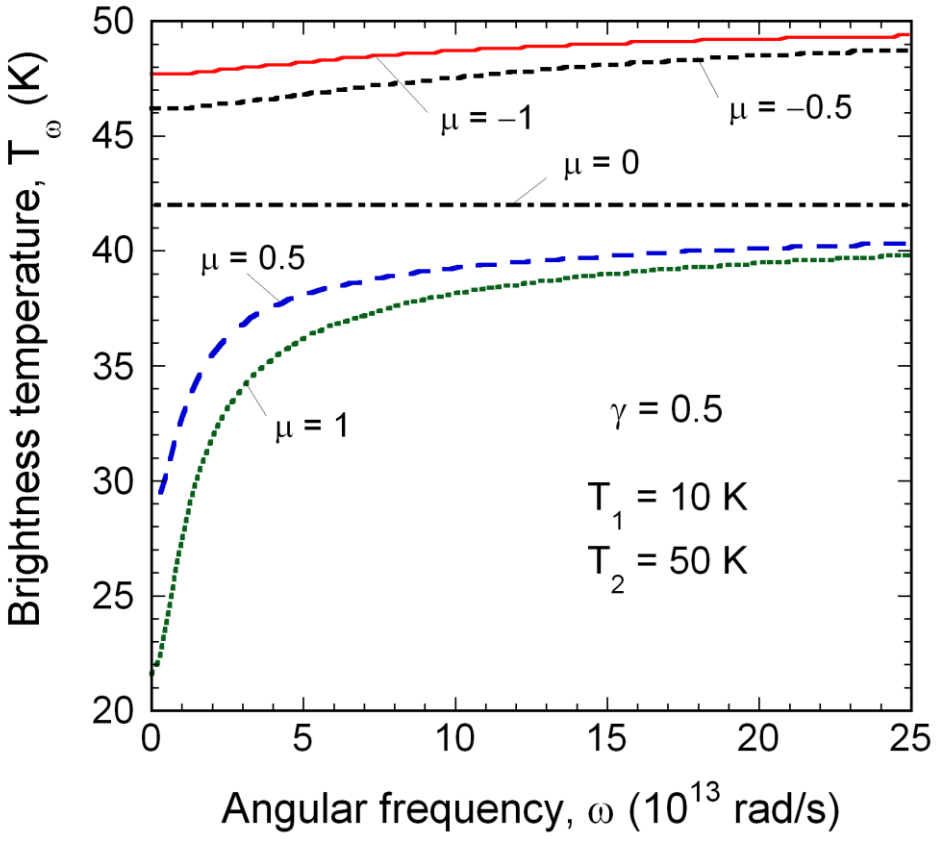

Fig. 4.6 Brightness temperature for different direction cosine in center of medium with $Kn = 1$ as a function of frequency.

Fig. 4.5. At any given frequency, the brightness temperature increases as θ is changed from 0 to 180° ($\mu = 1$ to -1). When $\mu = 0$, the brightness temperature is not a function of frequency and is equal to the effective temperature of the medium, T^*. Furthermore, at any given μ that is not equal to zero, the brightness temperature increases with increasing frequency. The fact that the brightness temperature is higher at higher frequencies is consistent with the plot shown in Fig. 4.1. It can be seen from Fig. 4.1 that at higher the frequency, the larger the relative difference between the averaged local intensity I_{avg} and the equilibrium intensity I_ω^0. At lower frequencies, I_{avg} becomes smaller than I_ω^0. From thermodynamic point of view, this suggests that more phonons at higher frequencies are absorbed than emitted, while at the same time more phonons at lower frequencies are emitted than absorbed. The absorption of higher-frequency phonons and emission of lower-frequency phonons is an irreversible process that is associated with entropy generation. It should be noted that, for gray medium, the absorption coefficient (which is inverse of the mean free path) is independent of frequency. Since the intensity is calculated from Eq. (4.8) and (4.9), the coupled absorption and emission processes result in the brightness temperatures at lower frequencies being closer to the medium temperature when $\mu < 0$. On the other hand, for $\mu > 0$, the brightness temperatures at higher frequencies are closer to the medium temperature. Since the effective thickness is $L/|\mu|$, in the direction normal to the wall, the effect of frequency on the brightness temperature is expected to be the largest. However, the variation of brightness temperature for $\mu < 0$ is not as large as for $\mu > 0$. It

turns out that the lower temperature side has a more prominent impact on the brightness temperature distribution, especially when $\mu = 1$.

In classical heat conduction, entropy flux can be expressed as

$$s_x''(x) = \frac{q_x''}{T^*(x)} \tag{4.29}$$

Equation (4.29) is not applicable inside the medium except in the diffusion limit. From the entropy intensity evaluated by using Eq. (4.18), the entropy flux inside the medium can be expressed as

$$s_x''(x) = 2\pi \int_0^{\omega_D} \int_{-1}^{1} L_\omega(\omega, \mu)\, \mu d\mu d\omega \tag{4.30}$$

The total entropy generation rate per unit area over the thickness L for heat conduction between two thermal reservoirs at T_1 and T_2 is

$$s_{tot}'' = q_x'' \left(\frac{1}{T_1} - \frac{1}{T_2} \right) \tag{4.31}$$

which is applicable for all thicknesses. Figure 4.7 shows the normalized entropy flux calculated from Eq. (4.30) for $T_1 = 10$ K and $T_2 = 50$ K. At the walls,

$$s_{w1}'' = \frac{q_x''}{T_1} \quad \text{and} \quad s_{w2}'' = \frac{q_x''}{T_2} \tag{4.32}$$

The increase in the entropy flux from right to left is caused by irreversibility inside the medium due to phonon radiative transfer. In fact, the integration of Eq. (4.20) from x_1 to x_2 is the same as the subtraction of the entropy flux, Eq. (4.30) at these two

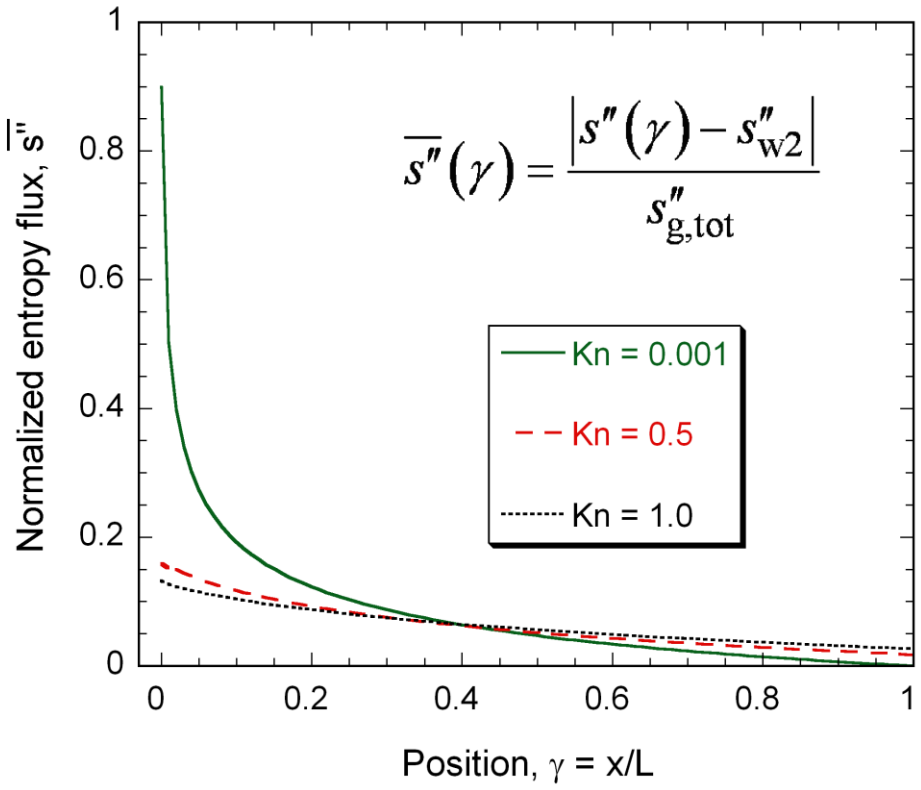

Fig. 4.7 Normalized entropy flux at different locations across the medium for different Kn. Note the jump at the walls corresponding to wall entropy generation.

locations. Furthermore, there is an entropy flux jump at the wall that represent the entropy generation by the wall as predicted by Eq. (4.21). It can be seen that the entropy generation is more significant towards the low temperature side. Furthermore, the entropy generation at the lower-temperature wall is much greater than at the higher-temperature wall. Even with $Kn = 0.001$ when the distance is 1000 times the mean free path, the entropy generation at the left wall is nearly 10% compared with the overall entropy generation.

Table 4.1 compares the entropy generation for different *Kn* at the walls and inside the medium. If the classical expression, Eq. (4.25), is used to calculate the medium entropy generation using the temperature solution from EPRT or the diffusion approximation with jump boundary conditions for small *Kn*, there will be a large error when *Kn* is large. Even when *Kn* is relatively small, e.g., $Kn = 0.1$, the difference can be as large as 15%. Note that one could simply use the entropy flux, Eq. (4.29), to calculate the conduction entropy generation inside the medium by

$$s''_{\text{gen,m}} = q''_x \left[\frac{1}{T^*(0)} - \frac{1}{T^*(L)} \right] \tag{4.33}$$

Table 4.1. Calculated entropy generation rate per unit area (W/K·m^2) between two black walls at temperatures $T_1 = 10$ K and $T_2 = 50$ K for various *Kn* for diamond. The relative difference in the medium entropy generation between the diffusion model and the radiation model is compared.

Kn	Medium (radiation)	Left Wall	Right Wall	Total	Medium (diffusion)	Relative Difference
1000	1.612E+04	2.320E+07	2.036E+06	2.524E+07	6.754E+03	58%
100	1.177E+05	2.297E+07	1.934E+06	2.503E+07	6.496E+04	45%
10	6.285E+05	2.109E+07	1.415E+06	2.314E+07	4.695E+05	25%
1	1.491E+06	1.211E+07	3.511E+05	1.395E+07	1.230E+06	17%
0.1	8.723E+05	2.080E+06	1.188E+04	2.964E+06	7.447E+05	15%
0.01	2.037E+05	1.272E+05	1.416E+02	3.311E+05	1.933E+05	5.1%
0.001	3.015E+04	3.389E+03	1.443E+00	3.354E+04	3.013E+04	0.07%
0.0001	3.323E+03	4.359E+01	1.445E-02	3.367E+03	3.315E+03	0.26%
0.00001	3.365E+02	4.501E-01	1.444E-04	3.369E+02	3.351E+02	0.40%

It is difficult to generalize the results presented in the table to different wall temperatures as they are presented as dimensional values. However, the same general trend is expected regardless of the wall temperatures. The general trend is a decrease in the difference between the radiation model and the conduction model as thickness of the medium is increased. Increasing medium thickness also results in the majority of entropy generation occurring inside of the medium and a decrease in the relative contribution of wall entropy generation. For all numerical integrations, a convergence criterion was used such that the relative difference between two iterations $\varepsilon_{\text{rel}} \leq 10^{-5}$ by mesh refinement. In the case of very small Kn (less than 0.001), the numerical calculation is based on the diffusion model with jump boundary conditions. In addition, the heat flux decreases as the thickness increases; thus reducing the numerical accuracy. Hence, the differences between the diffusion model and the radiation model in bottom two rows in Table 4.1 are presumably due to numerical error.

CHAPTER 5

CONCLUSIONS

The hyperbolic heat equation is fundamentally inconsistent with statistical mechanics and the solutions may violate the laws of thermodynamics. The claim that HHE can be validated by BTE is misleading since the assumptions made during the derivation invalidates its application to time scales shorter than the relaxation time, for which HHE was intended. While Fourier's law has its own limitations, HHE does not extend Fourier's law to describe the heat transfer process at short time scales, as it was originally proposed and believed by many heat transfer researchers. The infinite speed of propagation of diffusion process is consistent with the statistical theory and, furthermore, Fourier's law predicts a very slow diffusion process that has been validated by numerous experimental observations. Thermal waves observed at low temperatures are associated with a different phenomena of two-relaxation times and does not serve as evidence of HHE. The two-temperature model for ultrafast laser heating of metals contains a pair of coupled PHEs and does not predict wavelike behavior. The few experiments that showed temperature waves at near room temperatures in nonhomogenous materials could not be reproduced by others. Furthermore, attempts to thermodynamically justify HHE have not themselves been justified, albeit the completeness and selfconsistency of these theories. It is hoped that this study will clarify some common misunderstandings about HHE in the heat transfer community to avoid similar pitfalls in the future.

An analytical derivation of the entropy generation of a diffusion process inside of a medium has been presented from the more fundamental BTE and the conditions for

heat transport by phonons to be treated as such have been determined. Furthermore the entropy generation mechanism during phonon transport has been explored in a fundamental manner by applying concepts from radiation heat transfer to phonon transport. The concepts of radiation entropy generation in a participating medium and the brightness temperature have been extended to the phonon radiative process and are useful concepts for understanding the fundamental heat transport mechanism. Solutions to the EPRT have been presented, in a novel manner using the concept of brightness temperature, which give insight into heat transport by phonon radiation and the analogy between phonons and photons has been revisited to offer a unique perspective. Differences between phonon radiation and photon radiation have been stressed including the meaning of temperature for phonon radiation. Numerical results showed that the disagreement between the diffusion approximation for entropy can give relative errors larger than 10% for Knudsen numbers as low as 0.1. Emphasis was placed on understanding the fundamental nature of heat transport processes in dielectric solids and the entropy generation as phonon energy is redistributed throughout a medium by phonon scattering processes.

Future directions related to this work in the modeling of non-Fourier heat transfer could involve comparison of results from careful molecular dynamics simulation to those predicted by EPRT and HHE to assess the validity of those models. In addition since reliability of electronic devices is an important issue the prediction of phase change or material properties based on non-equilibrium temperatures as modeled by non-Fourier equations needs to be investigated. Furthermore techniques for reliably measuring the non-equilibrium temperatures need to be developed (if possible). An analysis of wall

entropy generation with realistic conditions such as the interface between two acoustically dissimilar thin film or a multilayer structure with different materials should be investigated to understand how real boundaries effect entropy production. Such an analysis could be coupled with models such as the acoustic and diffuse mismatch models or more sophisticated models to determine the transmissive and reflective properties of such an interface to give a more realistic surface model. Investigation of electronic transport in the non-Fourier regime and the interaction between electrons and phonons are promising areas of research and extension of the radiation model needs to be investigated.

REFERENCES

[1] Cattaneo, C., 1958, "Sur Une Forme De L'équation De La Chaleur Eliminate Le Paradoxe D'une Propagation Instantée," Comptes Rendus de l'Académie des Sciences, **247**, pp. 431-432.

[2] Vernotte, M.P., 1958, "Les Paradoxes De La Théorie Continue De L'équation De La Chaleur," Comptes Rendus de l'Académie des Sciences, **246**, pp. 3154-3155.

[3] Joseph, D.D., and Preziosi, L., 1989, "Heat Waves," Reviews of Modern Physics, **61**, pp. 41-73.

[4] Özisik, M.N., and Tzou, D.Y., 1994, "On the Wave Theory in Heat Conduction," Journal of Heat Transfer, **116**, pp. 526-535.

[5] Sharma, K.R., 2007, "Damped Wave Conduction and Relaxation in Cylindrical and Spherical Coordinates," Journal of Thermophysics and Heat Transfer, **21**, pp. 688-693.

[6] Tzou, D.Y., 1997, *Macro- to Microscale Heat Transfer : The Lagging Behavior*, Taylor & Francis, Washington, DC.

[7] Majumdar, A., 1993, "Microscale Heat Conduction in Dielectric Thin Films," Journal of Heat Transfer, **115**, pp. 7-16.

[8] Chen, G., 2005, *Nanoscale Energy Transport and Conversion : A Parallel Treatment of Electrons, Molecules, Phonons, and Photons*, Oxford University Press, New York.

[9] Zhang, Z.M., 2007, *Nano/Microscale Heat Transfer*, McGraw-Hill, New York.

[10] Taverneir, J., 1962, "Sur L'équation De Conduction De La Chaleur," Comptes rendus de l'Académie des sciences, **254**, pp. 69-71.

[11] Liboff, R.L., 2003, *Kinetic Theory : Classical, Quantum, and Relativistic Descriptions*, 3rd ed., Springer, New York.

[12] Kittel, C., 2005, *Introduction to Solid State Physics*, 8th ed., Wiley, New York.

[13] Casimir, H.B.G., 1938, "Note on the Conduction of Heat in Crystals," Physica, **5**, pp. 495-500.

[14] Joshi, A.A., and Majumdar, A., 1993, "Transient Ballistic and Diffusive Phonon Heat Transport in Thin Films," Journal of Applied Physics, **74**, pp. 31-39.

[15] Chen, G., 2001, "Ballistic-Diffusive Heat-Conduction Equations," Physical Review Letters, **86**, pp. 2297-2300.

[16] Xu, J., and Wang, X., 2004, "Simulation of Ballistic and Non-Fourier Thermal Transport in Ultra-Fast Laser Heating," Physica B: Condensed Matter, **351**, pp. 213-226.

[17] Özisik, M.N., and Vick, B., 1984, "Propagation and Reflection of Thermal Waves in a Finite Medium," International Journal of Heat and Mass Transfer, **27**, pp. 1845-1854.

[18] Tzou, D.Y., 1991, "The Resonance Phenomenon in Thermal Waves," International Journal of Engineering Science, **29**, pp. 1167-1177.

[19] Körner, C., and Bergmann, H.W., 1998, "The Physical Defects of the Hyperbolic Heat Conduction Equation," Applied Physics A: Materials Science & Processing, **67**, pp. 397-401.

[20] Bai, C., and Lavine, A.S., 1995, "On Hyperbolic Heat Conduction and the Second Law of Thermodynamics," Journal of Heat Transfer, **117**, pp. 256-263.

[21] Barletta, A., and Zanchini, E., 1997, "Hyperbolic Heat Conduction and Local Equilibrium: A Second Law Analysis," International Journal of Heat and Mass Transfer, **40**, pp. 1007-1016.

[22] Alvarez, F.X., Casas-Vazquez, J., and Jou, D., 2008, "Robustness of the Nonequilibrium Entropy Related to the Maxwell-Cattaneo Heat Equation," Physical Review E (Statistical, Nonlinear, and Soft Matter Physics), **77**, p. 031110.

[23] Jou, D., Casas-Vázquez, J., and Lebon, G., 2001, *Extended Irreversible Thermodynamics*, 3rd ed., Springer, New York.

[24] Onsager, L., 1931, "Reciprocal Relations in Irreversible Processes. I," Physical Review, **37**, pp. 405-426.

[25] Fujimoto, J.G., Liu, J.M., Ippen, E.P., and Bloembergen, N., 1984, "Femtosecond Laser Interaction with Metallic Tungsten and Nonequilibrium Electron and Lattice Temperatures," Physical Review Letters, **53**, pp. 1837-1840.

[26] Guyer, R.A., and Krumhansl, J.A., 1964, "Dispersion Relation for Second Sound in Solids," Physical Review, **133**, p. A1411.

[27] Guyer, R.A., and Krumhansl, J.A., 1966, "Solution of the Linearized Phonon Boltzmann Equation," Physical Review, **148**, pp. 766-778.

[28] Tang, D.W., and Araki, N., 1999, "Wavy, Wavelike, Diffusive Thermal Responses of Finite Rigid Slabs to High-Speed Heating of Laser-Pulses," International Journal of Heat and Mass Transfer, **42**, pp. 855-860.

[29] Kaminski, W., 1990, "Hyperbolic Heat Conduction Equation for Materials with a Nonhomogenous Inner Structure," Journal of Heat Transfer, **112**, pp. 555-560.

[30] Carslaw, H.S., and Jaeger, J.C., 1959, *Conduction of Heat in Solids*, 2nd ed., Clarendon Press, Oxford,.

[31] Incropera, F.P., and DeWitt, D.P., 2002, *Fundamentals of Heat and Mass Transfer*, 5th ed., Wiley, New York.

[32] Mitra, K., Kumar, S., Vedevarz, A., and Moallemi, M.K., 1995, "Experimental Evidence of Hyperbolic Heat Conduction in Processed Meat," Journal of Heat Transfer, **117**, pp. 568-573.

[33] Herwig, H., and Beckert, K., 2000, "Experimental Evidence About the Controversy Concerning Fourier or Non-Fourier Heat Conduction in Materials with a Nonhomogeneous Inner Structure," Heat and Mass Transfer, **36**, pp. 387-392.

[34] Bejan, A., 2006, *Advanced Engineering Thermodynamics*, 3rd ed., Wiley, New York.

[35] Planck, M., 1959, *The Theory of Heat Radiation*, Dover Publications, New York.

[36] Oxenius, J., 1966, "Radiative Transfer and Irreversibility," Journal of Quantitative Spectroscopy and Radiative Transfer, **6**, pp. 65-91.

[37] Kröll, W., 1967, "Properties of the Entropy Production Due to Radiative Transfer," Journal of Quantitative Spectroscopy and Radiative Transfer, **7**, pp. 715-723.

[38] Caldas, M., and Semiao, V., 2005, "Entropy Generation through Radiative Transfer in Participating Media: Analysis and Numerical Computation," Journal of Quantitative Spectroscopy and Radiative Transfer, **96**, pp. 423-437.

[39] Zhang, Z.M., and Basu, S., 2007, "Entropy Flow and Generation in Radiative Transfer between Surfaces," International Journal of Heat and Mass Transfer, **50**, pp. 702-712.

[40] Siegel, R., and Howell, J.R., 2002, *Thermal Radiation Heat Transfer*, 4th ed., Taylor & Francis, New York.

[41] Modest, M.F., 2003, *Radiative Heat Transfer*, 2nd ed., Academic Press, Boston.

[42] Little, W.A., 1959, "The Transport of Heat between Dissimilar Solids at Low Temperatures," Canadian Journal of Physics, **37**, pp. 334-349.

[43] Bright, T.J., and Zhang, Z.M., 2009, "Common Misperceptions of the Hyperbolic Heat Equation," Journal of Thermophysics and Heat Transfer, **23**, (in press).

[44] Prasher, R., 2003, "Phonon Transport in Anisotropic Scattering Particulate Media," Journal of Heat Transfer, **125**, pp. 1156-1162.

[45] Arpaci, V.S., 1987, "Radiative Entropy Production--Lost Heat into Entropy," International Journal of Heat and Mass Transfer, **30**, pp. 2115-2123.

[46] Liu, L.H., and Chu, S.X., 2006, "On the Entropy Generation Formula of Radiation Heat Transfer Processes," Journal of Heat Transfer, **128**, pp. 504-506.

[47] Deissler, R.G., 1964, "Diffusion Approximation for Thermal Radiation in Gases with Jump Boundary Condition," Journal of Heat Transfer, **86**, pp. 240-246.